

1 A hydrogeologic framework for characterizing
2 summer streamflow sensitivity to climate
3 warming in the Pacific Northwest, USA

4 Mohammad Safeeq^{1*}, Gordon E. Grant², Sarah L. Lewis¹, Marc G. Kramer^{3,4}, and Brian Staab³

5 ¹College of Earth, Ocean, and Atmospheric Sciences, Oregon State University, Corvallis, OR
6 97331

7 ²USDA Forest Service, PNW Research Station, Corvallis, OR 97331;

8 ³USDA Forest Service, PNW Region, Portland, OR 97208;

9 ⁴Current address: Soil and Water Science Department, University of Florida, Gainesville, FL
10 32611

11
12
13 *Corresponding author: Mohammad.Safeeq@oregonstate.edu, (541) 750-7345

14

15 **Abstract**

16 Summer streamflows in the Pacific Northwest are largely derived from melting snow and
17 groundwater discharge. As the climate warms, diminishing snowpack and earlier snowmelt will
18 cause reductions in summer streamflow. Most regional scale assessments of climate change
19 impacts on streamflow use downscaled temperature and precipitation projections from General
20 Circulation Models (GCMs) coupled with large scale hydrologic models. Here we develop and
21 apply an analytical hydrogeologic framework for characterizing summer streamflow sensitivity
22 to a change in the timing and magnitude of recharge in a spatially-explicit fashion. In particular,
23 we incorporate the role of deep groundwater, which large scale hydrologic models generally fail
24 to capture, into streamflow sensitivity assessments. We validate our analytical streamflow
25 sensitivities against two empirical measures of sensitivity derived using historical observations
26 of temperature, precipitation, and streamflow from 217 watersheds. In general, empirically and
27 analytically derived streamflow sensitivity values correspond. Although the selected watersheds
28 cover a range of hydrologic regimes (e.g. rain-dominated, mixture of rain and snow, and snow-
29 dominated), sensitivity validation was primarily driven by the snow dominated watersheds,
30 which are subjected to a wider range of change in recharge timing and magnitude as a result of
31 increased temperature. Overall, two patterns emerge from this analysis: first, areas with high
32 streamflow sensitivity also have higher summer streamflows as compared to low sensitivity
33 areas. Second, the level of sensitivity and spatial extent of highly sensitive areas diminishes over
34 time as the summer progresses. Results of this analysis point to a robust, practical, and scalable
35 approach that can help assess risk at the landscape scale, complement the downscaling approach,
36 be applied to any climate scenario of interest, and provide a framework to assist land and water
37 managers in adapting to an uncertain and potentially challenging future.

38 **Keywords:** Climate Change; Streamflow; Groundwater Processes; Pacific Northwest; Snowpack

39

40 1 Introduction

41 A fundamental challenge facing scientists and resource managers alike is grounding predictions
42 of climate change and its consequences in specific landscapes and at scales useful for resource
43 planning. This challenge is particularly acute for predictions of water abundance and scarcity, as
44 both the climatic and landscape controls on water availability are typically at a finer scale than
45 representations in the current class of climate and hydrologic models. Resource managers are
46 tasked to plan for an uncertain future by assessing vulnerabilities and sensitivities of different
47 landscapes to change. What strategy should they follow?

48 One way to assess streamflow vulnerability to changing climate is via a “top-down” approach,
49 which generally involves coupling General Circulation Models (GCMs) with hydrologic models
50 that predict regional streamflow (e.g. Nash and Gleick, 1991; Hamlet and Lettenmaier, 1999;
51 Nijssen et al., 2001; Christensen et al., 2004; Jha et al., 2004; Milly et al., 2005; Jha et al., 2006;
52 Tohver et al., 2014). This approach has many strengths, including simulation of hydrologic
53 processes under multiple climatic scenarios and across large spatial and temporal scales, and
54 forecasting hydrographs. But there are also limitations. GCMs coarsely parameterize terrain and
55 fail to incorporate important climatic processes, such as the El Niño/Southern Oscillation and
56 Pacific Decadal Oscillation, in predictions. Higher-resolution Regional Circulation Models
57 (RCMs) that include better topographic representation are improving this situation (Leung and
58 Qian, 2003; Maraun et al., 2010), but accurate forecasts of future climate by this method are still
59 several years off. Moreover, large scale hydrologic models commonly used in the Pacific
60 Northwest (PNW) for hydrologic forecasting (e.g. Variable Infiltration Capacity (VIC) (Liang et
61 al., 1994), do not explicitly simulate streamflow contributions from deep aquifers (Wenger et al.,
62 2010). However, the issue of deep-groundwater representation is not limited to VIC alone.
63 Explicit representation of deep-groundwater is approximated by extended soil profiles in many
64 large scale land surface models (Vano et al., 2012).

65 Several recent studies have demonstrated the important role of geologically-controlled deep
66 groundwater in mediating streamflow response to climatic variability and warming in the PNW
67 (Jefferson et al., 2008; Tague et al., 2008; Tague and Grant, 2009; Mayer and Naman, 2011;
68 Tague et al., 2013; Waibel et al., 2013). Historical streamflow analysis across the western United
69 States underscores the importance of both climatic and geologic controls on streamflow response
70 to climate change (Safeeq et al., 2013). Accordingly, approaches that capture both climate and
71 geologic controls are needed to identify landscape level streamflow vulnerability to changing
72 climate. This is particularly critical in the PNW, where local climate, topography and geology
73 combine to dictate hydrologic regimes.

74 In the PNW, seasonal asynchrony between winter and spring precipitation and runoff and
75 summer water demand makes summer water supplies scarce and vulnerable (Jaeger et al., 2013).
76 Climate change will intensify this water scarcity by reducing summer streamflows (Safeeq et al.,
77 2013). Declines have the potential to be acute, due to a combination of observed and predicted
78 shifts in precipitation phase from snow to rain, earlier onset and faster rates of snowmelt, and
79 increased summer evapotranspiration (Mote et al., 2005; Stewart et al., 2005; Nolin and Daly,
80 2006; Das et al., 2011). Increasing inter-annual variability and changes in extreme flows
81 compound seasonal changes. Luce and Holden (2009), for example, documented widespread
82 declines in the lowest annual flows occurring from 1948-2009; these flows are critical for

83 consumptive water use, hydropower, and aquatic biota, including the region’s prized and
84 declining salmon populations.

85 We present a complementary “bottom-up” approach, focusing on the PNW. Our methodology
86 rests on the analytical framework of Tague and Grant (2009) that characterizes relative summer
87 streamflow sensitivity. Using a rigorous definition of summer streamflow sensitivity as function
88 of the first derivatives of the relationship between discharge and either the timing or magnitude
89 of recharge, we develop a spatial analysis that characterizes summer streamflow sensitivity at a
90 landscape scale. Relationships between observed climate and streamflows at specific gaged
91 locations in diverse hydrogeologic areas are used to extend the sensitivity relationships to
92 ungaged areas and map sensitivity for the entire study region. The uniqueness and strength of
93 this approach is that it is independent of climate change scenarios. Sensitivity is mapped as an
94 intrinsic property of the landscape as interpreted using the average historical climate and other
95 landscape properties, rather than as a response to future climate change alone.

96 This sensitivity assessment can then be integrated with climate scenario data to produce regional-
97 scale summer streamflow vulnerability maps. We present an example of how this type of spatial
98 analysis might be applied to National Forest lands in the Pacific Northwest. Land and water
99 managers can tune this type of assessment to their specific needs in order to identify and
100 prioritize actions to adapt to uncertain and potentially challenging future conditions.

101 **2 Study Location**

102 This analysis encompasses Oregon (OR) and Washington (WA) in the northwestern United
103 States (US) with a population of nearly 10.5 million (US Census Bureau, 2010). The elevation
104 varies from sea level to over 4300 m at Mount Rainier, with the north-south trending mountains
105 of the Cascade Range dividing the western and eastern portions of the states (Fig. 1a). The study
106 region is divided into thirteen physiographic sections (Fig. 1b) based on common topography,
107 rock type, structure, and geomorphic history (Fenneman and Johnson, 1946). The maritime
108 climate is highly influenced by the Pacific Ocean and varies with elevation and distance from the
109 coast (Fig. 1b, 1c). Long-term average precipitation ranges from 150 mm in the Columbia Valley
110 on the eastside of the Cascades to ~7000 mm in the Olympic Mountains (Daly et al., 2008, Fig.
111 1c). Both OR and WA have extreme wet (winter) and dry (summer) seasons, but the seasonal
112 distribution of precipitation varies between the region’s eastern and western halves. While most
113 of the annual precipitation occurs during fall and winter, more frequent summer thunderstorms in
114 the eastern half result in a slightly higher summer precipitation (Mass, 2008). An altitudinal
115 temperature gradient, varying by latitude (Fig. 1c), controls the phase of precipitation with winter
116 rain (R) in lower elevations, seasonal snow at higher elevations (SSZ), and transient snow at
117 intermediate elevations (TSZ) (Jefferson, 2011). The majority of the winter precipitation occurs
118 as rain in the Coast Range and as snow along the Cascades and other ranges (e.g., Wallowa and
119 Blue Mountains).

120 This strong climatic gradient and underlying geology that mediate landscape drainage efficiency
121 (Tague and Grant, 2009) are predominant controls on the hydrologic regime of this region
122 (Wigington et al., 2013). For example, streamflow recedes quickly in watersheds with low spring
123 snowmelt and minimal groundwater storage (e.g., the OR Coast Range and western side of the
124 Middle Cascade Mountains (e.g. Western Cascades)), resulting in higher winter peaks and

125 prolonged summer low flows. In contrast, streams in groundwater-dominated regions such as the
 126 volcanic dominated central and eastern portion of the Middle Cascade Mountains (High
 127 Cascades) show a much more uniform flow regime, with higher summer baseflows, slower
 128 recession rates, and significantly lower winter peak flows (Grant, 1997; Tague and Grant, 2004).

129 **3 Conceptual Model of Streamflow Sensitivity**

130 Our conceptual model is built around the assumption that the discharge from a watershed
 131 depends solely on the amount of aquifer storage. Based on conservation of mass, the water
 132 balance within the watershed is given by:

$$133 \quad \frac{dS}{dt} = I_R + I_M + GW_{in} - ET - Q - GW_{out} \quad (1)$$

134 where, S is water stored in watershed (mm), I_R is rainfall (mm/day), I_M is snowmelt (mm/day),
 135 ET is evapotranspiration (mm/day), Q is discharge (mm/day), and GW_{in} and GW_{out} are the
 136 groundwater (mm/day) inflow and outflow, respectively. Change in storage (dS/dt) is positive
 137 when $I_R + I_M + GW_{in} - GW_{out} - ET > Q$ and negative whenever $Q > I_R + I_M + GW_{in} - GW_{out} - ET$.
 138 Maximum aquifer storage ($dS/dt = 0$) occurs when $Q = I_R + I_M + GW_{in} - GW_{out} - ET$, which should
 139 coincide with peak discharge ($dQ/dt = 0$) based on the storage-discharge relationship. In reality,
 140 since peak discharge always lags the peak recharge (Kirchner, 2009), the peak of the hydrograph
 141 will occur when $I_R + I_M + GW_{in} - GW_{out} - ET < Q$ and thus $dS/dt < 0$. However, we simplify and
 142 assume that at the peak of the hydrograph $dS/dt \approx 0$ and hence $Q \approx I_R + I_M + GW_{in} - GW_{out} - ET$ and
 143 equation (1) can be simplified to:

$$144 \quad Q_o = I_R + I_M + GW_{in} - ET - GW_{out} \quad (2)$$

145 where, Q_o is peak discharge (mm).

146 The recession curve of the hydrograph, or decay of Q_o over time, can be expressed by:

$$147 \quad Q(t) = Q_o e^{-kt} \quad (3)$$

148 where, $Q(t)$ is streamflow at time t (in days) from the beginning of the recession period, Q_o is
 149 streamflow at $t = 0$, and k is a recession constant (Tallaksen, 1995). As the climate warms, any
 150 change in the timing and magnitude of Q_o will affect $Q(t)$. Additionally, the recession time t
 151 depends on the day of the peak discharge t_p and the day t_d on which Q is quantified. Hence a
 152 more general form of equation (3) can be written as:

$$153 \quad Q(\Delta Q_o, t_s) = (Q_o + \Delta Q_o) e^{-k(t_d - t_p - t_s)} \quad (4)$$

154 where, ΔQ_o and t_s are change in peak discharge rate and shift in time driven by climate change,
 155 respectively. An earlier shift in peak discharge will result in a negative t_s and hence an overall
 156 longer recession period between t_p and the day t_d . Following Tague and Grant (2009), streamflow
 157 sensitivities to a shift in magnitude (ΔQ_o) and timing (t_s) can be described using a first order
 158 derivative of Eq. (4) with respect to peak discharge Q_o and time t :

$$159 \quad \frac{dQ(t)}{dQ_o} = \epsilon_{Q_o} = e^{-kt} \quad (5)$$

160
$$\frac{dQ(t)}{dt} = -\varepsilon_t = -kQ_0 e^{-kt} \quad (6)$$

161 where, terms ε_{Q_0} and ε_t represent the metrics used in this study to describe the sensitivity of
 162 discharge to changes in magnitude of peak discharge and timing, respectively. The negative sign
 163 in Eq. (6) indicates that $Q(t)$ decreases with increasing t .

164 The response surfaces of ε_{Q_0} and ε_t (Fig. 2) illustrate the interaction between t and k and how the
 165 two sensitivities are expressed over the course of the streamflow recession. In groundwater
 166 dominated systems with low values of k (e.g. High Cascades), ε_{Q_0} starts higher at the beginning
 167 of the recession and shows a very subtle decline with increasing t (Fig. 2a). In contrast, in the
 168 runoff dominated systems with high k (e.g. Western Cascades), ε_{Q_0} is very comparable to low k
 169 systems but diminishes very rapidly with increasing t . In the context of climate change, this
 170 suggests that while changes in summer streamflow in groundwater and runoff dominated systems
 171 with similar t_p and Q_0 may be comparable in the beginning of recession, they vary drastically as
 172 the recession progresses. The interaction between t and k for ε_t is more complex as compared to
 173 ε_{Q_0} (Fig. 2b). In groundwater dominated systems with low k , ε_t starts low and shows a very subtle
 174 decline with increasing t . In runoff dominated systems with high k , ε_t starts high but diminishes
 175 very quickly with increasing t . The very subtle and rapid decline of sensitivities (ε_{Q_0} and ε_t)
 176 between groundwater and runoff dominated systems expressed by the conceptual model are
 177 consistent with those expressed in streamflow trends in the empirical record. In groundwater
 178 dominated systems streamflow response to decreasing snowpack is mediated and streamflow
 179 continues to decline throughout the summer (Mayer and Naman, 2011; Safeeq et al., 2013).

180 Although our conceptual model of streamflow sensitivity is consistent with trends shown in the
 181 empirical streamflow record, we recognize that the complexity of the real world is not captured
 182 by this simple formulation. Hence, several caveats and assumptions must be emphasized when
 183 applying this model. While there is a physical basis for the conceptual model, it is not physically-
 184 based in a rigorous sense and involves several simplifying assumptions. Watersheds do not
 185 typically behave like linear reservoirs; filling (recharge) and emptying (discharge) often occur
 186 simultaneously, even during recession periods. Also groundwater exchange (GW_{in} and GW_{out})
 187 between watersheds dictates the streamflow regime in some parts of the landscape (Jefferson et
 188 al., 2006; Wigington et al., 2013; Patil et al., 2013). Physically accounting for groundwater gain
 189 and loss in this conceptual sensitivity framework with little or no data to draw on undermines the
 190 simplicity of this approach but introduces some error in some landscapes, notably those with
 191 large groundwater systems in young volcanic terranes. Additionally, this sensitivity approach
 192 assumes that Q_0 and t are independent and any change in Q_0 will not affect t . This assumption
 193 may hold true in rain dominated systems but could be problematic in snowmelt driven
 194 environments. However, this is a much less an issue in our study domain, where most of the
 195 snowmelt occurs during spring and summer recession characteristics depend primarily on peak
 196 initial recharge (Q_0). Additionally, approximating the I_R or I_M for Q_0 and t_R or t_M for t_p , even
 197 when $ET \approx 0$ and $GW_{in} = GW_{out}$ (Eq. 2) could result in biased estimates of sensitivity described in
 198 equations 5 and 6. In places where the reservoir is large, Q_0 gets delayed following recharge I_R or
 199 I_M , and t_R or t_M may not represent t_p . For example, in watersheds within the seasonal snow zone
 200 (see Section 4.2 for the definition), t_p is on average delayed by six days from t_M (Fig. 3). In rain
 201 dominated watersheds, the time lag between t_R and t_p is on average nine days for the first peak as

202 streamflow recovers from the long summer recession. This time lag between rainfall and
203 streamflow decreases to one or two days for the subsequent peaks (Fig. 3a, 3c). Although the
204 time lag between peak recharge and streamflow may vary significantly depending on data (e.g.
205 observed vs. simulated I_M and t_M) and method (e.g. isotopic techniques vs. simple recharge-
206 runoff relationship) used to characterize the relationship, our goal here is to highlight the issue
207 and how it might affect the sensitivity expressed using the conceptual model. Finally, the
208 watershed recession constant, k , may vary year-to-year depending on evapotranspiration losses
209 and other forms of water withdrawals (Thomas et al., 2013), which are not explicitly considered
210 in the model. Given these limitations, our intent is not to precisely predict the change in actual
211 flow regimes, but to assess the comparative sensitivity of those flow regimes across the
212 landscape.

213 **4 Parameterizing the Model**

214 **4.1 Recession Constant (k)**

215 Daily average streamflow data for a set of 227 (111 in OR and 116 in WA) unregulated
216 watersheds were obtained from the United States Geologic Survey (USGS)
217 (<http://waterdata.usgs.gov/or/nwis/sw>; data accessed on October 31, 2011) and the Oregon
218 Department of Water Resources (http://apps2.wrd.state.or.us/apps/sw/hydro_report/; data
219 accessed on November 1, 2011) (Fig. 1a). Watershed drainage areas range from 4 – ~21000 km²
220 with an average of approximately 950 km². These watersheds were classified as part of the
221 USGS Hydroclimatic Climatic Data Network (HCDN) (Slack et al., 1993), or were part of the
222 reference gage network developed by Falcone et al. (2010) based on Geospatial Attributes of
223 Gages for Evaluating Streamflow (GAGES). Both the HCDN and GAGES datasets have been
224 screened to ensure that they are minimally affected by upstream anthropogenic activities such as
225 irrigation diversions, road networks, and reservoir operations. To minimize the effect of climate
226 bias (i.e., wet vs. dry years) on estimates of k , all selected watersheds were further screened to
227 have a minimum of 20 years of complete daily streamflow data within the water years 1950–
228 2010. Since the majority of the streamflow gages were located in the western half of the study
229 area (Fig. 1a), we added 12 additional non-reference, non-HCDN gages to the eastern side to
230 ensure a more uniform population of basins. These 12 gages were selected after visual
231 examination of the historic streamflow data records for homogeneity, and review of site
232 information, including hydrologic disturbance index (Falcone et al., 2010) to ensure there were
233 no major diversions or impoundments. The selected 227 watersheds were delineated using a
234 30 m resolution digital elevation model (DEM).

235 **4.1.1 Recession analysis**

236 Following Vogel and Kroll (1992), an automated recession algorithm was employed to search
237 the historical record of daily streamflows for all recession segments lasting 10 days or longer.
238 Peak and end of recession segments were defined as when the 3-day moving average streamflow
239 began to recede and rise, respectively. The beginning of recession (inflection point) was
240 identified following the method of Arnold et al. (1995). To minimize the effect of snowmelt on
241 k , and thereby derive estimates of k that were intrinsic to the geology of the watershed, we
242 excluded recession segments that fell between the onset of snowmelt-derived streamflow pulse
243 and August 15th. We used August 15th as a cutoff for melt-out date determined based on
244 snowpack data from snowpack telemetry (SNOTEL) sites in OR and WA. The date of snowmelt

245 pulse onset was determined following the method of Cayan et al. (2001) and mean flow for
246 calendar days 9–248 after Stewart et al. (2005). Similar to Vogel and Kroll (1992), spurious
247 observations were avoided by only accepting pairs of receding streamflow (Q_t, Q_{t-1}) when $Q_t >$
248 $0.7Q_{t-1}$. The recession constant k was calculated as:

$$249 \quad k = \exp \left[\frac{1}{m} \sum_{t=1}^m \{ \ln(Q_{t-1} - Q_t) - \ln[0.5(Q_t + Q_{t+1})] \} \right] \quad (7)$$

250 where m is the total number of pairs of consecutive daily streamflow, Q_t and Q_{t-1} , at each site.
251 Among the 227 watersheds, the values of m varied between 24 and ~8000 (average ~3000).
252 Importance of k in characterizing the low flow behavior of streams has long been recognized but
253 there is a considerable debate on appropriate techniques for recession analysis (Tallaksen, 1995;
254 Vogel and Kroll, 1996; Smakhtin, 2001; Sujono et al., 2004). Estimates of k are comparable
255 using some techniques (Sujono et al., 2004) but not others (Vogel and Kroll, 1996). To ensure
256 that our k estimates for the candidate sites are robust and were not influenced by our choice of
257 the technique for recession analysis, we recalculated k from the master recession curve generated
258 for each site using the matching strip method (Posavec et al., 2006). We also calculated average
259 k from semi-logarithmic plots of individual recession segments lasting 10 days or longer during
260 non-snowmelt period as described earlier. The recession constant derived from the three methods
261 showed a strong correlation ($R > 0.77, p < 0.001$). We used the recession constant k from Eq. (7)
262 in the sensitivity analysis.

263 **4.1.2 Regression model development**

264 We established a regression model for transferring k to the ungaged landscape. Average
265 watershed relief and slope were estimated from a 30-m DEM using the ArcGIS spatial analyst.
266 Soil permeability (K_{soil} , cm/hr) values for the top 10 cm soil depth were obtained from the
267 STATSGO database (Miller and White, 1998; available online: <http://www.cei.psu.edu>). A
268 digital 1:500,000 scale ArcGIS coverage of aquifer permeability (K_{aqu} , m/day) derived from
269 existing aquifer unit maps for eastern OR (Gonthier, 1985) and western OR (McFarland, 1983)
270 was obtained from Wigington et al. (2013). Because this K_{aqu} dataset was not available for WA,
271 we developed a geologic index (ranging from 1 to 9 with higher values corresponding to higher
272 permeability) for OR and WA based on a 1:500,000-scale aquifer porosity and rock unit map
273 (Hunting et al., 1961; Walker et al., 2003). A regression between drainage densities estimated
274 using the National Hydrography Dataset (NHD) flowlines and the area-weighted geologic index
275 was used to assign the K_{aqu} values to each geologic index in WA. Area-weighted values of
276 average relief, slope, K_{soil} , and K_{aqu} were determined and log-transformed prior to the regression
277 analysis.

278 Starting with the entire list of parameters (i.e., relief, slope, K_{soil} , and K_{aqu}) from 227 watersheds,
279 we developed a multiple linear regression model. The established regression model was then
280 used to generalize k values across the region (wall-to-wall) at the landscape scale. The prediction
281 for k was made at the 5th field Hydrologic Unit Code (HUC) scale of the national Watershed
282 Boundary Dataset; 5th field HUC units are termed watersheds and typically range in area from
283 160 to 1010 km². Outliers in the model parameters were identified based on Cook's distance
284 (Cook, 2000) and subsequently excluded from the regression analysis using the recommended
285 threshold of $4/n_s - n_i - 1$, where n_s is the sample size and n_i is the number of independent variables.
286 Non-significant ($p \geq 0.15$) model parameters were then eliminated via backward stepwise
287 regression, until all remaining parameters were significant and the predictive power of the

288 equation (based on adjusted R^2) began to decline. This regression equation was developed
289 individually for OR and WA as well as the entire domain with both states combined (Table 1).
290 The correlation matrix for the watershed parameters used for predicting k showed strong cross-
291 correlation (as high as 0.72), particularly among K_{aqu} , Slope, and K_{soil} in OR. However, since
292 these variables are used to predict k and not to characterize their relationship with each other, the
293 cross-correlation and sign of the regression coefficients can be ignored.

294 The regression coefficients (R^2) for the three geographic domains (OR: Model 1a, WA: Model
295 1b, or OR and WA combined: Model 2) ranges between 0.44 for WA and 0.59 for OR (Table 1),
296 which are within the range of values reported elsewhere with a different set of independent
297 variables (e.g. Thomas et al., 2013). The overall standard error of the estimate is low for the
298 fitted regressions, and modeled k is only slightly biased, over-predicting small values and under-
299 predicting higher values of k (Fig. 4). There is no clear spatial pattern of systematic bias based on
300 residuals, however (Fig. 4d). The predicted k map using Model 2 at the 5th field HUC scale
301 broadly distinguishes among different hydrologic regions with different drainage characteristics,
302 including fast-draining regions such as the OR Coast Range, parts of the Columbia River Basin
303 in OR and WA and the Owyhee uplands and much of the Ochoco Mountains in OR. Slower-
304 draining regions include the eastern (High) Cascades in OR and WA and the Okanogan
305 highlands in WA (Fig. 5a), but the Okanogan k values are at the high end of the range for this bin
306 (0.02-0.04).

307 **4.2 Historical Recharge Magnitude and Timing (Q_o , t_p)**

308 We approximated the peak discharge (Q_o) in Eq. (2) by peak recharge (I_R or I_M depending on the
309 dominant recharge type), ignoring the groundwater exchange between HUC units ($GW_{\text{in}} = GW_{\text{out}}$
310 ≈ 0) and with $ET \approx 0$ at the start of the recession. In the PNW, the peak recharge pulse during the
311 water year can be either rain or snowmelt, depending on geographic location. We assigned the
312 primary type of peak recharge pulse (rain or snowmelt) based on a temperature threshold and
313 snow to precipitation proportion. Following Jefferson (2011) and Nolin and Daly (2006), a
314 winter temperature-based threshold of 0°C was chosen to approximate the boundary between the
315 transitional snow zone (TSZ) and rain zone, while -2°C was chosen to approximate the
316 boundary between the seasonal snow zone (SSZ) and TSZ. Following Knowles et al. (2006), we
317 define winter as beginning in November, rather than January, and only use wet-day minimum
318 temperatures, which showed a strong correlation with the snow to precipitation ratio. We defined
319 a wet-day as a day when daily precipitation is greater than zero. In addition, we used the
320 temperature threshold-based empirical relationship of Dai (2008) and the United States Army
321 Corps of Engineers (USACE, 1956) to calculate the median value (water year 1916-2006) of the
322 fraction of annual precipitation falling as snow. We classified the peak recharge pulse as rain for
323 the entire area within the identified rain zone and the portion of area in TSZ with a median snow
324 fraction $<10\%$; the remaining TSZ and entire SSZ were classified as snowmelt recharge pulse
325 (Fig. 5b).

326 A lack of spatially-distributed precipitation gauge and snowpack telemetry sites, particularly at
327 higher altitudes, precluded using empirical data to calculate recharge magnitude and timing.
328 Instead, we calculated the peak recharge magnitude (I_R and I_M) and timing (t_R and t_M) using
329 spatially distributed gridded ($1/16^{\text{th}}$ degree resolution) daily precipitation and VIC simulated
330 daily snowmelt data from Hamlet et al. (2013). The simulated snowmelt data from Hamlet et al.,
331 (2013) were limited to the Columbia River Basin and coastal river basins of OR and WA and did

332 not include the OR portions of the Klamath and Great Basins. VIC simulated daily snowmelt
 333 data for the Klamath and Great Basins at 1/8 degree spatial resolution were obtained from the US
 334 Bureau of Reclamation (Reclamation, 2011). VIC uses a two-layer energy and mass balance
 335 approach to model the process of snow accumulation and melt; descriptions of snow
 336 accumulation and melt processes within the VIC model are well described elsewhere (Liang et
 337 al., 1994; Ni-Meister and Gao, 2011).

338 The daily (1-365) average (1916-2006) maximum one-day recharge, I_R and I_M were calculated
 339 on the water year basis as:

$$340 \quad I_R = \max \left(\frac{\sum_{i=1}^N R_{i,1}}{N}, \frac{\sum_{i=1}^N R_{i,2}}{N}, \dots, \dots, \frac{\sum_{i=1}^N R_{i,365}}{N} \right) \quad (8)$$

$$341 \quad I_M = \max \left(\frac{\sum_{i=1}^N M_{i,1}}{N}, \frac{\sum_{i=1}^N M_{i,2}}{N}, \dots, \dots, \frac{\sum_{i=1}^N M_{i,365}}{N} \right) \quad (9)$$

342 where, R is the daily precipitation (mm), M is the daily snowmelt (mm), and N is the length of
 343 record (year). The corresponding timing t_R and t_M were calculated as the day of water year on
 344 which I_R and I_M occurred.

345 The spatial distribution of recharge magnitude (I_R and I_M) and timing (t_R and t_M) show distinct
 346 geographic contrasts between the eastern and western study domains (Fig. 6). The average peak
 347 daily recharge from precipitation (I_R) varies from less than 5 mm/day in the Walla Walla Plateau
 348 and much of eastern OR to as high as 44 mm/day in the Olympic Mountains to the west.
 349 Similarly, the average daily peak snowmelt (I_M) varies between 0 in coastal southeastern OR to
 350 as much 40 mm/day in northern WA. Although the magnitudes of I_R and I_M are small in north-
 351 eastern WA and much of eastern OR as compared to those in the Coast Range, northern WA, and
 352 Cascades, they occur later during the water year. In northern WA, the timing of I_M occurs quite
 353 late during the water year (Fig. 6). Timing of I_R is also quite variable across the region and
 354 occurs as early as October to as late as mid-September (Fig. 6). For the sensitivity analysis, in
 355 systems with rain as dominant recharge we substituted Q_o with I_R and t_p with t_R . Similarly, in
 356 systems with snowmelt as dominant recharge we substituted Q_o with I_M and t_p with t_M .

357 **4.3 Future Recharge Magnitude and Timing (Q_o , t_p)**

358 Changes in actual streamflow in the future will not only depend on the intrinsic sensitivity of the
 359 landscape but also the magnitude and direction of climate change in terms of magnitude (I_R or
 360 I_M) and timing (t_R or t_M) of recharge to which a landscape is exposed. The actual exposure or
 361 magnitude of change in I_R or I_M and t_R or t_M will depend on future emission scenarios, which are
 362 highly uncertain. However, to illustrate this concept of intrinsic sensitivity and exposure, we
 363 present a climate change scenario consistent with regional-scale climate projections for the PNW
 364 of decreasing snowpacks (Mote, 2003; Elsner et al., 2010) as a proxy for exposure. An integrated
 365 daily snow product based on the 1-km resolution Snow Data Assimilation System (Carroll et al.,
 366 2001) was selected and I_M and t_M were calculated as described earlier. We used the differences
 367 between I_M and t_M values for the wet year 2004 (an El Niño year) and dry year 2011 (a La Niña
 368 year), which correspond to a ~50% regional snowpack decline, as a potential climate change
 369 scenario. Changes in precipitation magnitude and timing are unclear for this region (Salathe et
 370 al., 2007; Mote and Salathe, 2010), and were excluded from this analysis.

371 5 Model Validation

372 We validated our derived streamflow sensitivities (ε_{Q_0} and ε_t) against empirical measures of
373 climate sensitivity extracted from historical records of 217 (Fig. 1a) watersheds for the months of
374 July, August, and September. Our approach was to use streamflow response to historical climate
375 extremes as a proxy for streamflow sensitivity. Measures used included the: 1) change in
376 streamflow with respect to a change in annual precipitation between wet and dry periods; and 2)
377 change in streamflow with respect to a change in spring air temperature between cool and warm
378 periods. These two empirical measures of sensitivity were calculated as:

$$379 \quad \varepsilon_p = \frac{Q_{\text{wet}} - Q_{\text{dry}}}{P_{\text{wet}} - P_{\text{dry}}} \quad (10)$$

$$380 \quad \varepsilon_T = \frac{Q_{\text{cool}} - Q_{\text{warm}}}{T_{\text{cool}} - T_{\text{warm}}} \quad (11)$$

381 Average annual precipitation (P) for each watershed was used to identify the 5 years with the
382 lowest and highest precipitation as dry and wet periods, respectively. Similarly, the watershed
383 average of mean daily spring (April - June) temperature (T) was used to identify the 5 years with
384 the coolest and warmest springs. This approach is analogous to the precipitation and temperature
385 elasticity measure of streamflow sensitivity proposed by Schaake (1990) and
386 Sankarasubramanian et al. (2001). The empirical measures ε_p and ε_T were calculated as an
387 indicator of streamflow sensitivity to a change in magnitude and timing of recharge, respectively.
388 However, magnitude (I_R and I_M) and timing (t_R and t_M) are each affected by wet and dry periods
389 and cool and warm springs (Table 2). Also, the effect of wet and dry climate on peak recharge
390 magnitude and timing differs for rain and snowmelt dominated systems. For example, during a
391 wet as compared to a dry period, t_M shifts 16 days later whereas t_R shifts 20 days earlier. Hence,
392 the empirical measures ε_p and ε_T are representative of the streamflow sensitivities as a
393 convolution of timing and magnitude. We used the non-parametric Spearman rank correlation (ρ)
394 coefficient to evaluate the correspondence between empirical (ε_p and ε_T) and conceptual (ε_{Q_0} and
395 ε_t) measures of streamflow sensitivities. Spearman rank correlation is less sensitive to outliers
396 and considered a robust alternative to the Pearson product moment correlation.

397 6 Results and Discussion

398 6.1 Sensitivity Validation

399 Summer streamflow sensitivities derived from the conceptual framework are in agreement with
400 the climate sensitivity estimators calculated from historical data (Table 2). The absolute
401 magnitudes of both empirical (ε_p and ε_T) and conceptual (ε_{Q_0} and ε_t) measures of streamflow
402 sensitivities decrease from July to September. Also, both precipitation- and temperature-based
403 estimators of streamflow sensitivity ε_p and ε_T are significantly ($p < 0.001$) correlated with ε_{Q_0} and
404 ε_t . The Spearman rank correlation coefficient for ε_p and ε_{Q_0} decreases from 0.73 in July to 0.50
405 in September, and for ε_p and ε_t decreases from 0.77 in July to 0.54 in September. The Spearman
406 rank correlations between ε_p and ε_{Q_0} or ε_t are weaker and ranged between -0.66 (ε_p vs. ε_{Q_0}) and -
407 0.71 (ε_p vs. ε_t) in July and -0.5 in September. The overall slightly lower values of Spearman rank
408 correlations between empirical and conceptual measures of streamflow sensitivities are not

409 surprising given the fact that changes in I_M and t_M between wet and dry periods were very small.
410 Similarly, between cool and warm periods I_R and t_R were relatively constant. So although we
411 used a total 217 watersheds for validation, not all of them were subjected to a change in
412 magnitude and timing of recharge between wet and dry or cool and warm periods. In fact, all of
413 the rain dominated watersheds had similar I_R and t_R between cool and warm periods. This
414 smaller change in I_R and t_R limits the range of our validation for rain dominated watersheds.

415 6.2 Sensitivity Analysis & Distribution

416 Streamflow sensitivities to a change in magnitude, ϵ_{Q_0} , are very similar during the first weeks
417 after peak recharge for all HUC units across the range of k values (Fig. 7a). In groundwater
418 dominated HUCs, the ϵ_{Q_0} are mediated and show very sharp contrasts from runoff dominated
419 HUCs even after 110 days of recession. Since peak recharge I_M occurs late during the year in
420 most of the low k HUCs (Fig. 6), these mediated sensitivities will be expressed throughout the
421 summer. In contrast, the sensitivities to a change in timing, ϵ_t , are very different during the first
422 weeks after peak recharge across all HUC units (Fig. 7b). Most of the HUCs with higher ϵ_t (>0.5
423 mm/day) are in the rain dominated Coast Range (Fig. 1) where recharge magnitude (I_R) is higher
424 overall when compared to the snow dominated Cascades, Olympics, and other western parts of
425 OR and WA. However, in most of these coastal HUCs the peak recharge occurs early in the year
426 (Fig. 6), resulting in a long recession with lower sensitivities in the summer months.

427 Summer streamflow sensitivities to a change in the magnitude (ϵ_{Q_0}) and timing (ϵ_t) of recharge at
428 the beginning of July, August, and September show several distinct patterns (Fig. 8). First, there
429 is a clear north-south grain to the sensitivity of both variables due primarily to the corresponding
430 orientation of the topography, with the Cascade Range in both OR and WA clearly showing up
431 as most sensitive to both types of changes. Snow-dominated regions with late melt, such as the
432 mountains along the WA-Canada border and the Willowa Mountains in OR also show a high,
433 though diminished, sensitivity. Second, the maps show that 5th field HUCs sensitive to a change
434 in magnitude (I_R and I_M) are also sensitive to a change in timing (t_R and t_M). Third, the level of
435 sensitivity and its spatial extent diminish as the day of interest (t_d) moves from early to late
436 summer. The highest magnitudes of sensitivity to changes in I_R and I_M , were 0.47, 0.25, and 0.14
437 mm/mm at the start of July, August, and September, respectively; The highest magnitudes of
438 sensitivity to changes in t_R and t_M were 0.28, 0.10, and 0.03 mm/day, at the start of July, August,
439 and September, respectively. The highest sensitivity for July streamflow is primarily located in
440 the northern WA and along the Cascades, but portions of OR Cascades continue to show high
441 sensitivity throughout the summer. This contrasting pattern is attributed to relatively high k
442 values in the OR Cascades compared to northern WA. By the end of August, OR Cascade
443 streams are mainly sourced from deep groundwater, as most of the above-ground storage in the
444 form of snow has melted out (Tague and Grant, 2004).

445 The influence of k becomes more important than peak recharge magnitude and timing as summer
446 proceeds. Thus, although the different regions display similar levels of sensitivity, the reasons for
447 this sensitivity vary by locale. In contrast, summer streamflow (i.e., July, August, and
448 September) in HUCs that receive recharge in the form of rain (e.g., Coast Range) and do not
449 have deep groundwater, are less sensitive to a change in the I_R or t_R compared to HUCs driven by
450 snowmelt recharge (e.g., High Cascade range and much of northern WA). This lower sensitivity
451 primarily results from peak rainfall occurring earlier in the year (Fig. 6), leading to a long

452 summer recession. A similar low sensitivity is observed in eastern OR, where peak snowmelt
453 occurs later in the year but the magnitude of recharge I_M is small and there is very little deep
454 groundwater contribution to sustain the recession.

455 Over the entire study area, streamflow at the start of July is at least moderately sensitive (ϵ_{Q_0} and
456 $\epsilon_t > 0.001$) to a change in peak recharge magnitude and timing in 49% and 27% of the area,
457 respectively. As the day of interest moves towards the start of September, the spatial extent of at
458 least moderately sensitive areas diminishes to 25% and 11% of the region for ϵ_{Q_0} and ϵ_t ,
459 respectively. Within the individual states, streamflow at the start of July in OR is at least
460 moderately sensitive in 38% and 16% of the area as compared to 64% and 44% of the area in
461 WA, to a change in peak recharge magnitude and timing, respectively. Similarly, streamflow at
462 the start of September in OR is at least moderately sensitive in 15% and 6% of the area as
463 compared to 39% and 18% of the area in WA, to a change in peak recharge magnitude and
464 timing, respectively.

465 **6.3 Summer Streamflow Vulnerability**

466 This analysis yields a spatially-explicit prediction of the sensitivity of late summer streamflow to
467 climate change based on the convolution of geology, as represented by k , and recharge dynamics,
468 as represented by I_R , I_M , t_R and t_M (Fig. 8). To better understand this sensitivity, we consider how
469 the processes driving it vary across the landscape. For example, the OR High Cascades and much
470 of WA show similar levels of sensitivity, but for different reasons. The OR High Cascades are
471 sensitive because of low k and, as a result, abundant deep, and slow draining groundwater that
472 recharges streams over many months. Peak snowmelt recharge, I_M in much of the OR Cascades
473 is not only small compared to northern WA, but also melts earlier (Fig. 6), leaving deep
474 groundwater as the only source of late season streamflow. These groundwater-dominated
475 landscapes in effect “remember” changes in climate as reflected in either the magnitude or
476 timing of recharge in the winter or spring, resulting in higher sensitivity of late-season
477 streamflow.

478 In contrast, much of northern WA is sensitive not because of low k but because of higher I_R or I_M
479 and late t_R and t_M . The I_M is higher in much of this region and melts later during the year (Fig. 6),
480 contributing a substantial portion of the late season streamflow. If the climate changes so that
481 less snow accumulates and snowmelt occurs earlier in spring, the corresponding changes in
482 recharge timing and magnitude are reflected in late summer streamflow, which relies almost
483 exclusively on snowmelt in this region.

484 The hydrogeologic sensitivities (Fig. 8) illustrate the magnitude of change to existing summer
485 streamflows during early July, August, and September, per unit change in recharge magnitude
486 and timing. Hence, the sensitivity is an intrinsic, mappable landscape property driven primarily
487 by current climate and geology. This information is valuable for climate change planning and
488 mitigation efforts, particularly in ungauged basins, which represent most of the landscape. Our
489 analysis predicts sensitivity to change, but not actual changes to magnitude or timing of
490 streamflow. Actual changes in summer streamflow are a product of both this hydrogeologic
491 sensitivity (Fig. 8) and realized changes in I_R or I_M and t_R or t_M under a given climate change
492 scenario. Changes in ET are also a factor, but are not considered here.

493 Summer streamflow change resulting from this test scenario can be expressed both in absolute
494 (units of flow increase or decrease over time) and relative (percentage increase or decrease over
495 time with respect to Q_0) terms, depending on the application and subject of interest. The average
496 change in I_M and t_M between the year 2004 and 2011 was 4.1 ± 4.5 mm and 38 ± 34 days,
497 respectively. We then calculated late summer streamflow at the beginning of July, August, and
498 September using the change in I_M and t_M values separately (Fig. 9). Only 7% of the region
499 showed a decline in July 1st streamflow by at least 1 mm (a threshold equivalent to average daily
500 September streamflow) under the I_M scenario as compared to 8% under the t_M scenario. Most of
501 the HUCs with a 1 mm or greater decline are located in WA. Nearly 16% of the area in WA
502 showed at least a 1 mm decline in July 1st streamflow as compared to only 3% in OR to a change
503 in t_M between the years 2004 and 2011. Similarly, 12% of the area in WA showed at least a 1 mm
504 decline in July 1st streamflow as compared to only 3% in OR to a change in I_M between the year
505 2004 and 2011. As expected, streamflow changes in July were larger than in August and
506 September under both the I_M (Fig. 9a) and t_M (Fig. 9b) scenarios. Relative changes (%) in
507 streamflow were calculated after normalizing the absolute change by the peak snowmelt recharge
508 (I_M) as a proxy for Q_0 . In the absence of spatially distributed observed streamflow data, we
509 utilized the peak recharge as a proxy for available water in the streams at the start of the
510 recession. In general, areas showing greater absolute change also showed greater relative change
511 (Fig. 9a, 9b).

512 This disparity between absolute and relative change across the landscape illustrates a key aspect
513 of interpreting sensitivity: our prediction of future streamflows reflects both the intrinsic
514 sensitivity of the landscape (as reflected in k and average historic climate) as well as changes in
515 snowpack between cooler and warmer years. Both factors affect the timing or magnitude of
516 recharge. Specifically, under our assumed scenario, the changes in I_M and t_M , are greater in
517 places with “warmer” snowpacks (Nolin and Daly, 2006), such as the Cascades and other
518 mountain ranges that are closer to marine influence (e.g., Olympics, Fig. 1b). In these areas,
519 small temperature changes directly affect the total proportion of snow to precipitation. In
520 contrast, colder snowpack areas such as the Harney and Great Basins, Payette, and Walla Walla
521 Plateau (Fig. 1b) are less sensitive to temperature changes. The net effect to streamflow is that
522 some regions (e.g. Northern Cascades, Fig. 1b) experience both more vulnerable snowpack and
523 more sensitive landscapes (i.e. lower k values). This is reflected in both a greater absolute and
524 relative change (Fig. 9). The drier eastern portions of the study region, in contrast, have lower
525 absolute change because their snowpacks are relatively insensitive to warming, and k values are
526 higher.

527 **7 Management Applications**

528 A central goal in developing this spatially-explicit, analytical framework was to help resource
529 managers, such as the US Forest Service (USFS), evaluate vulnerabilities of key resources to
530 changing summer streamflows, and develop and implement adaption strategies to reduce
531 potential impacts. While such strategies may introduce some new activities (e.g., facilitated
532 migration of species, mulching forests) (Grant et al., 2013), we expect that most will involve
533 adjustments in the location, timing, and scope of current actions or modification of their site-
534 specific designs.

535 To explore this, we consider how this type of spatial analysis might inform management of
536 National Forest lands in the Pacific Northwest. National Forests comprise a particularly large
537 fraction of the region (nearly 27 % of OR and WA) and support diverse, valuable, and climate-
538 sensitive resources. The largest changes in summer streamflows are expected to occur on these
539 forest lands, which may affect and alter numerous forest management activities. Such activities
540 include timber harvest and fuels management, watershed restoration, resource assessment and
541 monitoring, and construction and operation of dams, water diversions, roads, and recreational
542 facilities.

543 Watershed restoration is currently a major focus for the USFS (Potyondy and Geier, 2011).
544 Much of this work in the Pacific Northwest is directed towards maintaining or improving water
545 quality and aquatic habitats for salmon and other cold water biota, as directed by the Northwest
546 Forest Plan and other forest plans in the region. Common restoration actions include removal of
547 physical barriers in streams (e.g., poorly designed culverts), road improvements and
548 decommissioning, improved livestock management, reconstruction of stream channels and
549 floodplains, restoration of riparian vegetation and streamflows, decommissioning or alteration of
550 dams and water diversions, and enhancement of instream habitats via additions of wood,
551 boulders, and nutrients (Roni et al., 2002).

552 Implementing these restoration projects in a ‘climate informed’ way is critical, as changes in
553 summer streamflows and other habitat components (e.g., stream thermal regimes) may
554 significantly influence their effectiveness (Battin et al., 2007). This can be accomplished by
555 integrating assessment products like the one presented here into existing strategic planning and
556 project design processes. For example, to maximize the effectiveness of its restoration program,
557 the USFS is currently focusing investments in ‘priority watersheds’ based on assessments of
558 non-climatic stressors and other factors (Watershed Condition Framework at
559 <http://www.fs.fed.us/publications/watershed/>). In the PNW, those watersheds where the greatest
560 ecological gains can be achieved with the least funding have typically been selected as priorities.
561 In general, such areas have high ecological values (e.g., high biodiversity, rare or legally
562 protected species), mild to modest levels of non-climatic impacts (e.g., water diversions, water
563 quality problems, altered stream habitats), high sensitivities to those impacts (e.g., cold water
564 biota with narrow thermal tolerances), and significant opportunities for restoration (e.g.,
565 important and technically-solvable problems, sufficient financial resources and workforce
566 capacity, community support, few legal barriers).

567 This sensitivity assessment provides an opportunity to consider an additional factor in the
568 priority-setting: climate-induced changes in summer streamflow. In many cases, such changes
569 may not alter priority areas selected for restoration. For example, current priority watersheds
570 may remain priorities after consideration of climate change information (Fig. 10). In others,
571 however, likely climate impacts may shift emphasis away from some watersheds and towards
572 others. For example, watersheds with large projected changes in summer streamflows and water
573 resources highly sensitive to those changes may be considered a lower restoration priority if
574 restoration treatments are unlikely to address the cumulative effects of both climatic and non-
575 climatic impacts or if the cost of those treatments greatly exceed available funding (i.e., adaptive
576 capacity is limited). Conversely, the relative priority of other watersheds may increase in cases
577 where significant climate impacts are expected, but managing both climatic and non-climatic
578 impacts is deemed technically, socially, and financially achievable (Fig. 10).

579 Moreover, this analysis could influence the type, intensity, location, or timing of restoration
580 actions considered necessary to sustain critical resources in priority watersheds, both at a
581 watershed and project scale. The prospect of late-season streamflow change in some portions of
582 the watershed could lead to redesign of water diversions, proactive efforts to reduce stream
583 temperatures, re-thinking low-flow channel dimensions for fish passage and stream channel
584 reconstruction projects, and reconsideration of what riparian species are likely to survive into the
585 future (Fig. 10).

586 **8 Conclusions**

587 Our results provide a hydrogeologic framework to identify watersheds most and least vulnerable
588 to summer streamflow changes. This method reveals landscape level patterns and their
589 relationship to topographic, geologic and climatic controls, and can be applied to interpret the
590 effects of any climate change scenario of interest. As such, we believe the sensitivity maps
591 represent a robust, scalable tool that can be used in climate change assessment and adaptation in
592 both gaged and ungauged basins.

593 Lack of geologic (i.e., aquifer permeability) and snowmelt information at appropriate spatial
594 scales and accuracies to predict drainage efficiency and peak recharge magnitude and timing is a
595 challenge. For example, aquifer permeability used for OR and WA at the scale of 1:500,000
596 reflects far less spatial heterogeneity and it is unclear how a finer scale (i.e., 1:100,000)
597 permeability or geology map would influence k . Similarly, we relied on simulated historic
598 snowmelt data at 1/16 and 1/8 degree grid resolution due to the absence of long-term, spatially-
599 distributed measurements. It is unclear how the changes in temperature and precipitation will
600 affect or assumption to approximate the peak discharge with recharge. As the climate continues
601 to warm, the time lag between recharge and streamflow (Fig. 3) in rain and snow dominated
602 watersheds will likely shift. More rain instead of snow will also alter the dominant recharge
603 regime (Fig., 5b) and eventually the streamflow sensitivities. Also, this sensitivity analysis
604 should be applied carefully in places where subsurface groundwater exchange or summer
605 evapotranspiration dominate summer streamflow regime. As finer-resolution data on both
606 geological and climatic factors becomes available, this approach can be refined to capture new
607 information.

608 More broadly, we recognize that this approach does not yield the specific streamflow values or
609 future hydrographs of the current generation of hydrologic models. There are many applications
610 where having a spatio-temporal prediction of how much water is present would be quite useful.
611 Beyond the uncertainty in both our approach and streamflow modeling, each method has
612 strengths and limitations. The spatial map of sensitivity reveals broad landscape patterns and is
613 applicable where data, time, or cost limit applying a more sophisticated hydrologic model.
614 Hydrologic models give detailed predictions, but may not always illuminate underlying
615 mechanisms or provide sound future predictions. Both approaches have their place. Although our
616 results are independent of GCM predictions, the two approaches are not necessarily mutually
617 exclusive. New CMIP5 high resolution, terrain sensitive model predictions could be incorporated
618 into this framework. .

619 Predicting future streamflows is an uncertain task at best, but is essential to address a rapidly
620 changing environment. The “bottom up” approach described here is intended to complement

621 other “top down” approaches involving sophisticated and coupled climate and hydrologic
622 models. These spatial maps based on simple theory and supported by empirical data represent
623 spatially-explicit hypotheses about how streamflow is expected to respond to climate changes in
624 the future. Other more complex approaches also yield spatially-explicit hypotheses in the form of
625 future hydrographs. We can now compare these two approaches, highlight their strengths and
626 limitations, and integrate knowledge from each to guide managers and communities in facing the
627 uncertain future of water resources in the Pacific Northwest and beyond.

628 **Acknowledgements**

629 The authors gratefully thank three anonymous reviewers for their helpful comments. They
630 acknowledge funding support from the Oregon Watershed Enhancement Board, the Bureau of
631 Land Management (Oregon) and the USDA Forest Service Region 6 and Pacific Northwest
632 Research Station.

633 **References**

- 634 Arnold, J.G., Allen, P.M., Muttiah, R., and Bernhardt, G., 1995. Automated base flow separation
635 and recession analysis techniques. *Ground Water* 33 (6):1010-1018.
- 636 Battin, J., Wiley, M.W., Ruckelshaus, M.H., Palmer, R.N., Korb, E., Bartz, K.K., and Imaki, H.,
637 2007. Projected impacts of climate change on salmon habitat restoration. *Proceedings of*
638 *the National Academy of Sciences of the United States of America* 104:6720–6725.
- 639 Carroll, T., Cline, D., Fall, G., Nilsson, A., Li, L., and Rost, A., 2001. NOHRSC operations and
640 the simulation of snow cover properties for the coterminous US. In: *Proceedings of the*
641 *69th Western Snow Conference*, pp 16-19.
- 642 Cayan, D.R., Kammerdiener, S.A., Dettinger, M.D., Caprio, J.M., and Peterson, D.H., 2001.
643 Changes in the onset of spring in the western United States. *Bulletin of the American*
644 *Meteorological Society* 82 (3):399-415.
- 645 Cook, R.D., 2000. Detection of influential observation in linear regression. *Technometrics* 42
646 (1):65-68.
- 647 Christensen, N.S., Wood, A.W., Voisin, N., Lettenmaier, D.P., and Palmer, R.N., 2004. The
648 effects of climate change on the hydrology and water resources of the Colorado River
649 basin. *Climatic change*, 62(1-3), 337-363.
- 650 Dai, A., 2008. Temperature and pressure dependence of the rain-snow phase transition over land
651 and ocean. *Geophys Res Lett* 35:L12802.
- 652 Daly, C., Halbleib, M., Smith, J.I., Gibson, W.P., Doggett, M.K., Taylor, G.H., Curtis, J., and
653 Pasteris, P.P., 2008. Physiographically sensitive mapping of climatological temperature
654 and precipitation across the conterminous United States. *International Journal of*
655 *Climatology* 28 (15):2031-2064.
- 656 Das, T., Pierce, D.W., Cayan, D.R., Vano, J.A., and Lettenmaier, D.P., 2011. The importance of
657 warm season warming to western U.S. streamflow changes. *Geophys Res Lett* 38 (23).
- 658 Elsner, M.M., Cuo, L., Voisin, N., Deems, J.S., Hamlet, A.F., Vano, J.A., Mickelson, K.E.B.,
659 Lee, S-Y, and Lettenmaier, D.P., 2010. Implications of 21st century climate change for
660 the hydrology of Washington State. *Clim Change* 102 (1-2):225-260.
- 661 Falcone, J.A., Carlisle, D.M., Wolock, D.M., and Meador, M.R., 2010. GAGES: A stream gage
662 database for evaluating natural and altered flow conditions in the conterminous United
663 States. *Ecology* 91 (2):621-621.

664 Fenneman, N.M., and Johnson, D.W., 1946, Physiographic Divisions of the United States, U.S.
665 Geological Survey (USGS), Washington, D.C., (available online:
666 http://water.usgs.gov/GIS/dsdl/physio_shp.zip , access date 07-07-2014).

667 Gonthier, J.B., 1985. A description of aquifer units in Eastern Oregon. US Geological Survey,
668 p357.

669 Grant, G.E., 1997. Dynamics and geomorphology of mountain rivers [Book Review]. *J N Am*
670 *Benthol Soc* 16:719-720.

671 Grant, G.E., Tague, C.L., and Allen, C.D., 2013. Watering the forest for the trees: an emerging
672 priority for managing water in forest landscapes. *Frontiers in Ecology and Environment*
673 11 (6): 314–321.

674 Hamlet, A.F., and Lettenmaier, D. P., 1999. Effects of climate change on hydrology and water
675 resources in the Columbia River Basin. *JAWRA Journal of the American Water*
676 *Resources Association* 35(6) 1597-1623.

677 Hamlet, A.F., Elsner, M.M., Mauger, G., Lee, S-Y, Tohver, I., and Norheim, R.A., 2013. An
678 overview of the Columbia Basin Climate Change Scenarios Project: Approach, methods,
679 and summary of key results. *Atmos Ocean* 51 (4) 392-415.

680 Hunting, M.T., Bennett, W.A.G., Livingston, V.E.J., and Moen, W.S., 1961. Geologic Map of
681 Washington: Washington Division of Mines and Geology, scale 1:500,000. online at
682 [:http://mrdata.usgs.gov/sgmc/wa.html](http://mrdata.usgs.gov/sgmc/wa.html).

683 Jaeger, W.K., Plantinga, A.J., Chang, H., Dello, K., Grant, G.E., Hulse, D., McDonnell, J.J.,
684 Lancaster, S., Moradkhani, H., Morzillo, A.T., Mote, P., Nolin, A., Santelmann, M., and
685 Wu, J., 2013. Toward a formal definition of water scarcity in natural human systems.
686 *Water Resources Research* 49 (7) 4506–4517.

687 Jefferson, A., Grant, G. and Rose, T., 2006. Influence of volcanic history on groundwater
688 patterns on the west slope of the Oregon High Cascades, *Water Resour. Res.*, 42,
689 W12411, doi:10.1029/2005WR004812.

690 Jefferson, A.J., Nolin, A.W., Lewis, S.L., and Tague, C.L., 2008. Hydrogeologic controls on
691 streamflow sensitivity to climate variation. *Hydrological Processes* 22 (22):4371-4385.

692 Jefferson, A.J., 2011. Seasonal versus transient snow and the elevation dependence of climate
693 sensitivity in maritime mountainous regions. *Journal of Geophysical Research* 38
694 (16):L16402. doi:10.1029/2011gl048346.

695 Jha, M., Pan, Z., Takle, E.S., and Gu, R., 2004. Impacts of climate change on streamflow in the
696 Upper Mississippi River Basin: A regional climate model perspective. *Journal of*
697 *Geophysical Research: Atmospheres* (1984–2012), 109(D9).

698 Jha, M., Arnold, J.G., Gassman, P.W., Giorgi, F., and Gu, R.R., 2006. Climate change
699 sensitivity assessment on upper mississippi river basin streamflows using SWAT.
700 *JAWRA Journal of the American Water Resources Association* 42(4) 997-1015.

701 Kirchner, J.W., 2009. Catchments as simple dynamical systems: Catchment characterization,
702 rainfall-runoff modeling, and doing hydrology backward. *Water Resources Research*, 45,
703 W02429, doi:10.1029/2008WR006912.

704 Knowles, N., Dettinger, M.D., Cayan, D.R., 2006. Trends in snowfall versus rainfall in the
705 Western United States. *Journal of Climate* 19:4545-4559.

706 Leung, L.R., and Qian, Y., 2003. The sensitivity of precipitation and snowpack simulations to
707 model resolution via nesting in regions of complex terrain. *Journal of Hydrometeorology*
708 4 (6):1025-1043.

709 Liang, X., Lettenmaier, D.P., Wood, E.F., and Burges, S.J., 199. A simple hydrologically based
710 model of land surface water and energy fluxes for general circulation models. *Journal of*
711 *Geophysical Research: Atmospheres* 99 (D7):14415-14428.

712 Luce, C.H., and Holden, Z.A., 2009. Declining annual streamflow distributions in the Pacific
713 Northwest United States, 1948–2006. *Geophys Res Lett* 36 (16).

714 Maraun, D., Wetterhall, F., Ireson, A.M., Chandler, R.E., Kendon, E.J., Widmann, M., Brienen,
715 S., Rust, H.W., Sauter, T., Themeßl, M., Venema, V.K.C., Chun, K.P., Goodess, C.M.,
716 Jones, R.G., Onof, C., Vrac, M., and Thiele-Eich, I., 2010. Precipitation downscaling
717 under climate change: Recent developments to bridge the gap between dynamical models
718 and the end user. *Rev Geophys* 48 (3):RG3003.

719 Mass, C., 2008. *The weather of the Pacific Northwest*. University of Washington Press Seattle,
720 Washington.

721 Mayer, T.D., and Naman, S.W., 2011. Streamflow response to climate as influenced by geology
722 and elevation. *JAWRA Journal of the American Water Resources Association* 47
723 (4):724-738.

724 McFarland, W.D., 1983. Description of aquifer units in western Oregon. Available from OFSS,
725 USGS Box 25425 Lakewood, CO 80225 USGS Open-File Report 82-165, 1983 35 p, 13
726 fig, 5 tab, 84 ref.

727 Miller, D.A., and White, R.A. 1998. A conterminous United States multilayer soil characteristics
728 dataset for regional climate and hydrology modeling. *Earth interactions*, 2, 1-26.

729 Milly, P.C., Dunne, K.A., and Vecchia, A.V., 2005. Global pattern of trends in streamflow and
730 water availability in a changing climate. *Nature*, 438(7066), 347-350.

731 Mote, P.W., 2003. Trends in snow water equivalent in the Pacific Northwest and their climatic
732 causes. *Geophys Res Lett* 30 (12).

733 Mote, P.W., Hamlet, A.F., Clark, M.P., and Lettenmaier, D.P., 2005. Declining mountain
734 snowpack in western North America. *Bulletin of the American Meteorological Society* 86
735 (1):39-49.

736 Mote, P.W., and Salathe, E. P., 2010. Future climate in the Pacific Northwest. *Climatic Change*,
737 102(1-2), 29-50.

738 Nash, L.L., and Gleick, P.H., 1991. Sensitivity of streamflow in the Colorado basin to climatic
739 changes. *Journal of hydrology*, 125(3), 221-241.

740 Ni-Meister, W., and Gao, H., 2011. Assessing the impacts of vegetation heterogeneity on energy
741 fluxes and snowmelt in boreal forests. *Journal of Plant Ecology* 4 (1-2):37-47.

742 Nijssen, B., O'Donnell, G.M., Hamlet, A.F., and Lettenmaier, D.P., 2001. Hydrologic sensitivity
743 of global rivers to climate change. *Climatic change*, 50(1-2), 143-175.

744 Nolin, A.W., Daly, C., 2006. Mapping "at Risk" snow in the Pacific Northwest. *Journal of*
745 *Hydrometeorology* 7:1164-1171.

746 Patil, S.D., Wigington, P.J., Leibowitz, S.G. and Comeleo, R.L. 2013. Use of hydrologic
747 landscape classification to diagnose streamflow predictability in Oregon. *JAWRA*
748 *Journal of the American Water Resources Association*, doi:10.1111/jawr.12143.

749 Posavec, K., Bačani, A., and Nakić, Z., 2006. A visual basic spreadsheet macro for recession
750 curve analysis. *Ground Water* 44 (5):764-767.

751 Potyondy, J.P., and Geier, T.W., 2011. *Watershed condition classification technical guide*,
752 United States Department of Agriculture, Forest Service, FS-978, July 2011.

753 Reclamation, 2011. SECURE Water Act Section 9503(c) – Reclamation Climate Change and
754 Water, Report to Congress, 2011.

755 Roni, P., Beechie, T.J., Bilby, R.E., Leonetti, F.E., Pollock, M.M., and Pess, G.R., 2002. A
756 review of stream restoration techniques and a hierarchical strategy for prioritizing
757 restoration in Pacific Northwest watersheds. *N Am J Fish Manage* 22 (1):1-20.

758 Safeeq, M., Grant, G.E., Lewis, S.L., and Tague, C.L., 2013. Coupling snowpack and
759 groundwater dynamics to interpret historical streamflow trends in the western United
760 States. *Hydrological Processes*. 27:655-668.

761 Salathe, E.P., Mote, P.W., and Wiley, M. W., 2007. Review of scenario selection and
762 downscaling methods for the assessment of climate change impacts on hydrology in the
763 United States Pacific Northwest. *International Journal of Climatology*, 27(12), 1611-
764 1621.

765 Sankarasubramanian, A., Vogel, R.M., and Limbrunner, J.F., 2001. Climate elasticity of
766 streamflow in the United States. *Water Resources Research* 37 (6):1771-1781.

767 Schaake, J.C., 1990. From climate to flow. *Climate change and US water resources*:177-206.

768 Slack, J.R., Lumb, A.M., and Landwehr, J.M., 1993. Hydroclimatic data network (HCDN): A U.
769 S. Geological Survey streamflow data set for the United States for the study of climate
770 variation, 1874– 1988. U.S. Geological Survey Water Resources Investigation Report 93-
771 4076.

772 Smakhtin, V.U., 2001. Low flow hydrology: a review. *Journal of Hydrology* 240: 147–186.

773 Stewart, I., Cayan, D.R., and Dettinger, M., 2005. Changes toward earlier streamflow timing
774 across western North America. *J Climate* 18:1136-1155.

775 Sujono, J., Shikasho, S., and Hiramatsu, K., 2004. A comparison of techniques for hydrograph
776 recession analysis. *Hydrological Processes* 18, 403–413.

777 Tague, C.L., Grant, G.E., Farrell, M., Choate, J., and Jefferson, A., 2008. Deep groundwater
778 mediates streamflow response to climate warming in the Oregon Cascades. *Clim Change*
779 86 (1-2):189-210.

780 Tague, C.L., and Grant, G.E., 2004. A geological framework for interpreting the low-flow
781 regimes of Cascade streams, Willamette River Basin, Oregon. *Water Resources Research*
782 40 (4).

783 Tague, C.L., and Grant, G.E., 2009. Groundwater dynamics mediate low-flow response to global
784 warming in snow-dominated alpine regions. *Water Resources Research* 45 (7).

785 Tague, C.L., Choate, J., Grant, G.E., 2013. Parameterizing sub-surface drainage with geology to
786 improve modeling streamflow responses to climate in data limited environments.
787 *Hydrology and Earth System Sciences* 17:341-354.

788 Tallaksen, L., 1995. A review of baseflow recession analysis. *Journal of Hydrology* 165 (1):349-
789 370.

790 Thomas, B.F., Vogel, R.M., Kroll, C.N., and Famiglietti, J.S., 2013. Estimation of the base flow
791 recession constant under human interference. *Water Resources Research*, 49(11), 7366-
792 7379.

793 Tohver, I.M., Hamlet, A F., and Lee, S.Y., 2014. Impacts of 21st-Century Climate Change on
794 Hydrologic Extreme in the Pacific Northwest Region of North America. *JAWRA Journal*
795 *of the American Water Resources Association*. DOI: 10.1111/jawr.12199

796 USACE, 1956. Snow hydrology summary report of the snow investigations of the North Pacific
797 Division, Portland, OR.

798 US Census Bureau, 2010. Population Division, also available online:
799 <http://www.census.gov/popest/estimates.html> (retrieved, October 10, 2011).

800 Vano, J.A., Das, T., and Lettenmaier, D. P., 2012. Hydrologic sensitivities of Colorado river
801 runoff to changes in precipitation and temperature. *Journal of Hydrometeorology*, 13,
802 932-949.

803 Vogel, R.M., and Kroll, C.N., 1992. Regional geohydrologic-geomorphic relationships for the
804 estimation of low-flow statistics. *Water Resources Research* 28 (9):2451-2458.

805 Vogel, R.M., and Kroll, C.N., 1996. Estimation of baseflow recession constants. *Water*
806 *Resources Management* 10:303-320.

807 Waibel, M.S., Gannett, M.W., Chang, H., and Hulbe, C.L., 2013. Spatial variability of the
808 response to climate change in regional groundwater systems – Examples from
809 simulations in the Deschutes Basin, Oregon. *Journal of Hydrology* 486:187-201.

810 Walker, G.W., MacLeod, N.S., Miller, R.J., Raines, G.L., and Connors, K.A., 2003. Spatial
811 digital database for the geologic map of Oregon. U.S. Geological Survey, Menlo Park,
812 California.

813 Wenger, S.J., Luce, C.H., Hamlet, A.F., Isaak, D.J., and Neville, H.M., 2010. Macroscale
814 hydrologic modeling of ecologically relevant flow metrics. *Water Resources Research* 46
815 (9).

816 Wigington, P.J., Leibowitz, S.G., Comeleo, R.L., and Ebersole, J.L., 2013. Oregon hydrologic
817 landscapes: a classification framework. *Journal of the American Water Resources*
818 *Association*. 49 (1)163–182
819

820

821

822

823

824

825 **Tables**

826 **Table 1:** Regression analysis for prediction of k in Oregon (*Model 1a*) and Washington (*Model*
 827 *1b*) and the entire domain (*Model 2*), using *relief*, soil permeability (K_{soil}), aquifer permeability
 828 (K_{aqu}) and *slope*.

	Regression Equation	d.f.	Se	R²	Adj. R²	F Statistics
<i>Model 1a</i>						
OR	$k = 0.2939448$					
	$-0.0272553 \log(\textit{Relief})$	97	0.010	0.59	0.58	45.39
	$-0.0118343 \log(K_{soil})$					
	$-0.0011999 \log(K_{aqu})$					
<i>Model 1b</i>						
WA	$k = 0.159973$					
	$-0.014864 \log(\textit{Relief})$	95	0.011	0.44	0.43	25.36
	$-0.012880 \log(K_{aqu})$					
	$+0.006182 \log(K_{soil})$					
<i>Model 2</i>						
Domain (OR & WA)	$k = 0.1942972$					
	$-0.0214605 \log(\textit{Relief})$	199	0.011	0.50	0.49	65.88
	$+0.0043926 \log(\textit{Slope})$					
	$-0.0027865 \log(K_{aqu})$					

d.f. is degree of freedom; Se is standard error.

829
 830
 831
 832
 833
 834
 835
 836
 837
 838

839 **Table 2:** Watershed average ($n = 217$) values of peak recharge magnitude and timing between
 840 wet/dry and cool/warm periods with corresponding empirical and analytically derived
 841 streamflow sensitivity values.

Scenario	Average Parameter Value				Empirical Validation			Derived Sensitivity		
	I_R (mm)	I_M (mm)	t_R (day)	t_M (day)	\mathcal{E}_P (mm/mm), Eq. 10			\mathcal{E}_{Q_0} (mm/mm), Eq. 5		
					July	Aug	Sep	July	Aug	Sep
Wet	35.95	6.95	86	167	0.046	0.016	0.013	0.046	0.017	0.0066
Dry	21.56	4.32	106	151						
	I_R (mm)	I_M (mm)	t_R (day)	t_M (day)	\mathcal{E}_T (mm/°C), Eq. 11			\mathcal{E}_t (mm/day), Eq. 6		
					July	Aug	Sep	July	Aug	Sep
	Cool	28.03	7.33	89	180	-22.17	-7.89	-2.89	0.014	0.004
Warm	28.13	4.56	87	154						

842

843

844 **Figures**

845

846 **Figure 1:** (A) Study domain and selected stream gages ($n = 227$; all circles) in Oregon and
847 Washington used to calculate k . Stream gages ($n = 217$; light blue circles) with at least 20 years
848 of daily streamflow between 1950 and 2010 were used in the sensitivity validation and other
849 time series comparisons of rain, snowmelt, and streamflow; (B) Physiographic regions based on
850 common topography, rock type, structure, and geomorphic history; (C) average (1981-2010)
851 annual precipitation; (D) average (1981-2010) temperature.

852 **Figure 2:** Theoretical response surface from conceptual model (Tague and Grant, 2009) for
853 representative k values for the study region. Sensitivity of summer streamflow to (A) a change in
854 the magnitude of recharge (mm/mm) and (B) an earlier shift in the timing of recharge (mm/day)
855 assuming an initial recharge volume of 1 mm.

856 **Figure 3:** Time series of daily rainfall (A), snowmelt (B), and streamflow (C) averaged over the
857 available lengths of record and n watersheds in rain (R, $n = 44$; green), transitional snow zone
858 (TSZ, $n = 43$; red), and seasonal Snow zone (SSZ, $n = 130$; blue). Solid lines represent the mean
859 value and shaded areas represent the standard error of the mean.

860 **Figure 4:** Calculated and modeled flow recession constant (k) for watersheds in (A) OR, (B)
861 WA, and (C) entire domain based on the regression equations developed individually for OR
862 (Model 1a), WA (Model 1b) and for the entire domain (Model 2)); (D) Spatial distribution of
863 residuals (Calculated-Modeled) using Model 2.

864 **Figure 5A:** Spatial distribution of recession constant k using Model 2 for the entire domain of
865 Oregon and Washington. Lower k values represent deep groundwater-dominated systems; higher
866 k values represent surface flow-dominated systems.

867 **Figure 5B:** Study domain discretized between rain (R; green), transitional snow zone (TSZ;
868 blue), and seasonal snow zone (SSZ; gray) based on Nov-Jan average wet day air temperature.
869 Areas in the TSZ with a snow to precipitation ratio (S_f) $>10\%$ are shaded with light blue.

870 **Figure 6:** Spatial distribution of peak recharge magnitude (mm/day) for precipitation I_R (a),
871 snowmelt I_M (b) and recharge timing (day of water year) for precipitation t_R (c) and snowmelt t_M
872 (d) across the study domain.

873 **Figure 7:** Decline of streamflow sensitivities for the range of k across all HUC units to a change
874 in (A) magnitude, ε_{Q_0} and (B) timing, ε_t during the first 110 days of recession from the peak
875 recharge, t_p . White shading indicates no data.

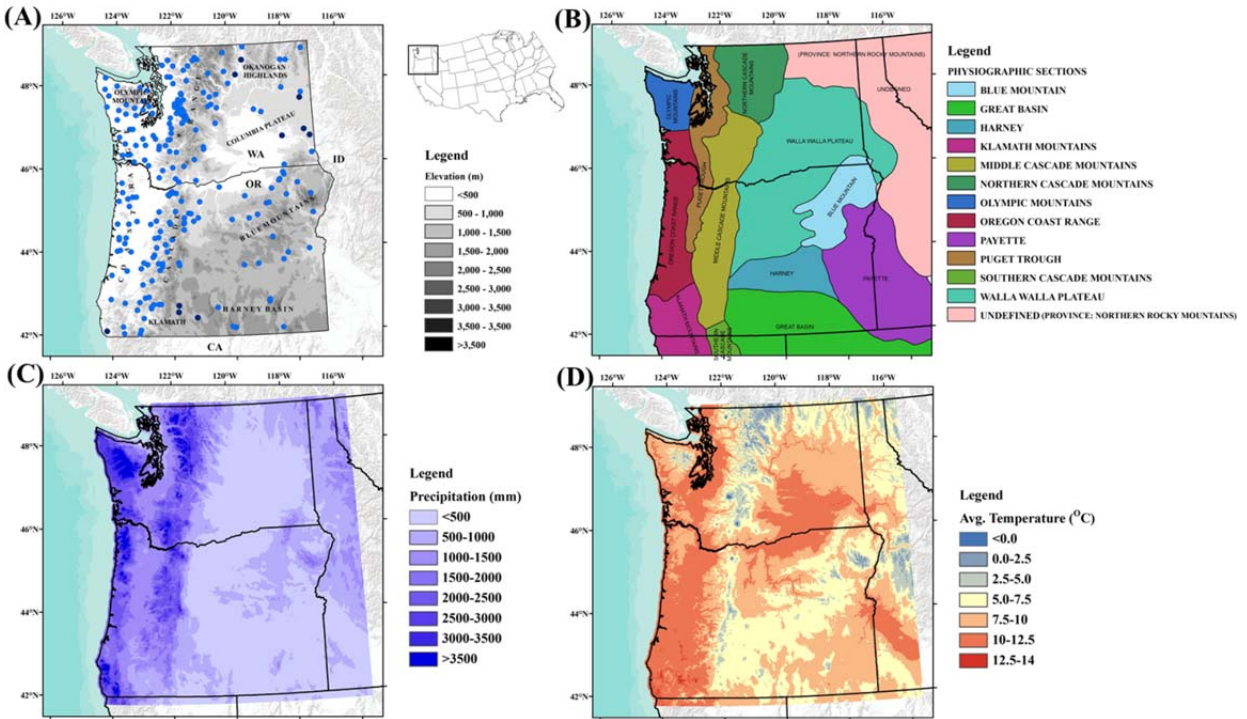
876 **Figure 8:** Spatial distribution of (A) July, (B) August and (C) September streamflow sensitivities
877 to a change in (i) magnitude ε_{Q_0} (mm/mm) and (ii) timing ε_t (mm/day) of recharge.

878 **Figure 9A:** Predicted decline in streamflow in absolute (i) and relative (ii) terms, based on: 1)
879 the intrinsic sensitivities to changes in peak snowmelt magnitude (Fig. 8); and 2) a scenario
880 similar to the differences experienced between a warm, dry year (2003, El Niño) and a cool, wet
881 year (2011, La Niña). Gray areas are rain dominated recharge and were excluded from this
882 analysis.

883 **Figure 9B:** Predicted decline in streamflow in absolute (i) and relative (ii) terms, based on: 1)
884 the intrinsic sensitivities to changes in peak snowmelt timing (Fig. 8); and 2) a scenario similar
885 to the difference experienced between a warm, dry year (2003, El Niño) and a cool, wet year
886 (2011, La Niña). Gray areas are rain dominated recharge and were excluded from this analysis.

887 **Figure 10:** Examples of hypothetical watershed prioritization based on USDA Forest Service
888 Watershed Condition Classification, an assessment of non-climatic impacts, sensitivities to those
889 impacts, and opportunities to address them. Priority watersheds (red stars) differ for
890 classifications without (A) and with (C) streamflow sensitivity analysis (B).

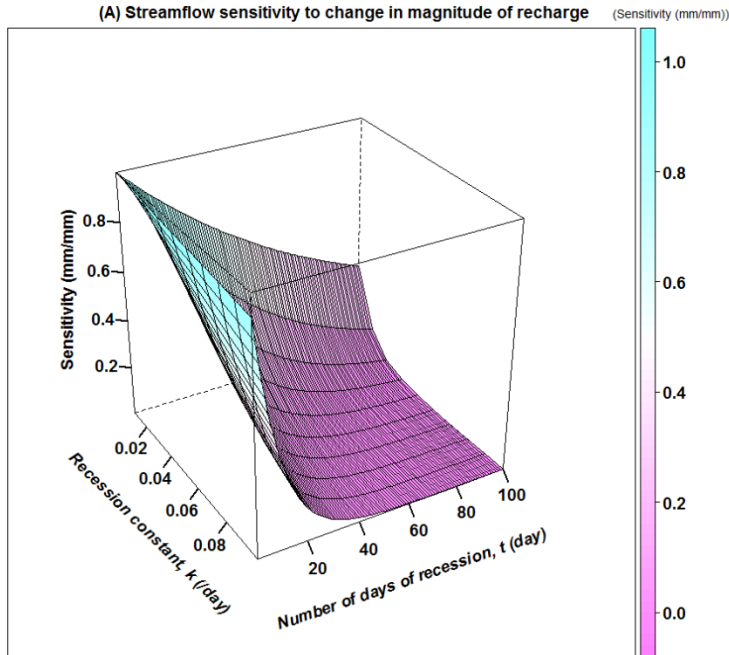
891



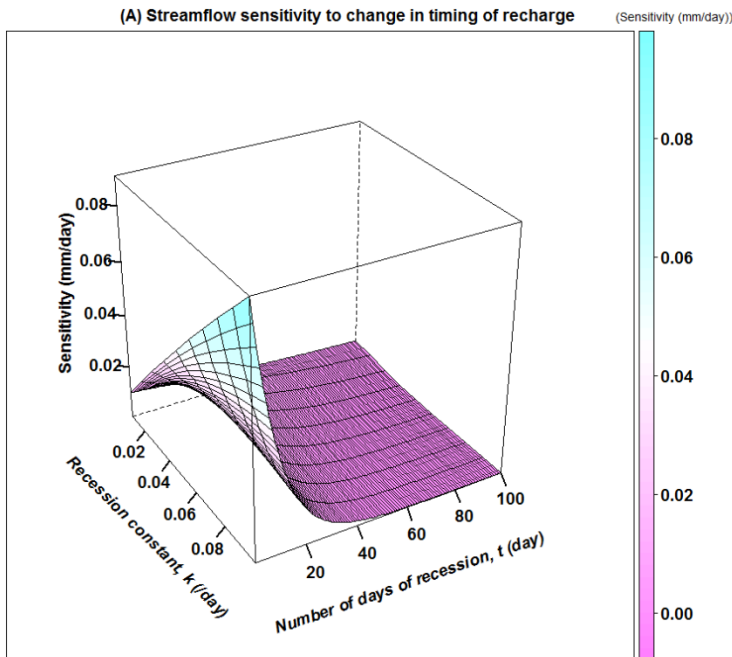
892

893 **Figure 1:** (A) Study domain and selected stream gages ($n = 227$; all circles) in Oregon and
 894 Washington used to calculate k . Stream gages ($n = 217$; light blue circles) with at least 20 years
 895 of daily streamflow between 1950 and 2010 were used in the sensitivity validation and other
 896 time series comparisons of rain, snowmelt, and streamflow; (B) Physiographic regions based on
 897 common topography, rock type, structure, and geomorphic history; (C) average (1981-2010)
 898 annual precipitation; (D) average (1981-2010) temperature.

899



900

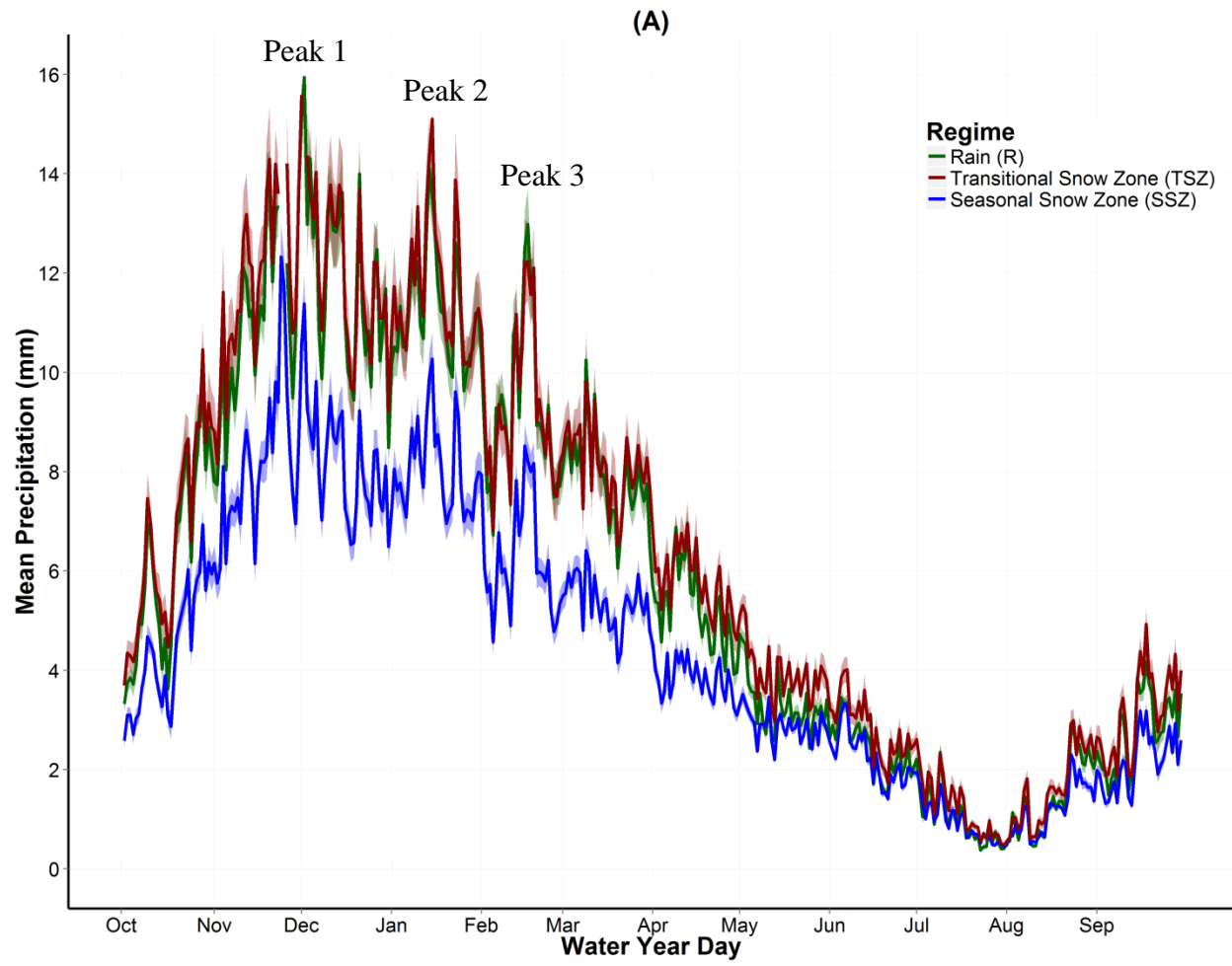


901

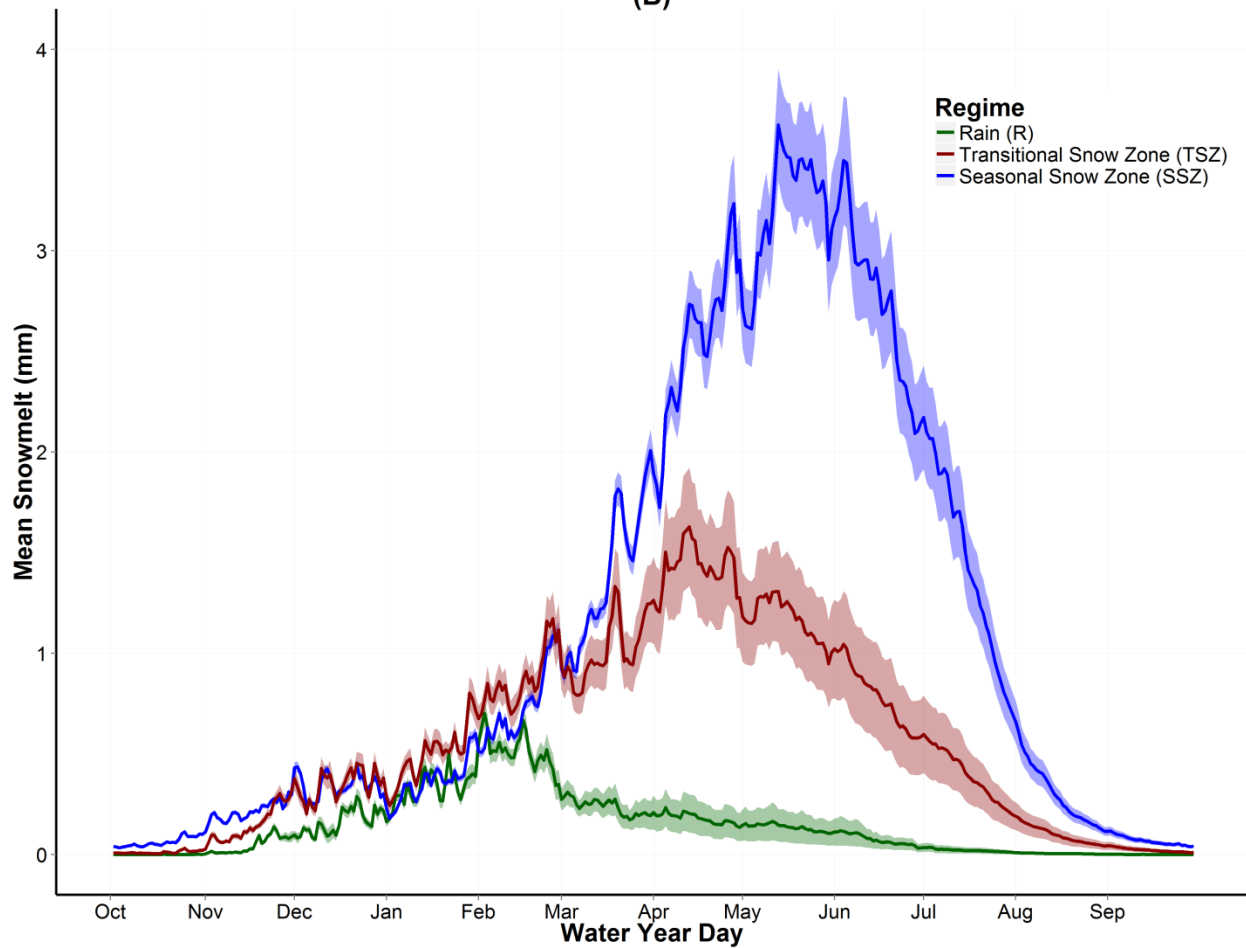
902 **Figure 2:** Theoretical response surface from conceptual model (Tague and Grant, 2009) for
 903 representative k values for the study region. Sensitivity of summer streamflow to (A) a change in
 904 the magnitude of recharge (mm/mm) and (B) an earlier shift in the timing of recharge (mm/day)
 905 assuming an initial recharge volume of 1 mm.

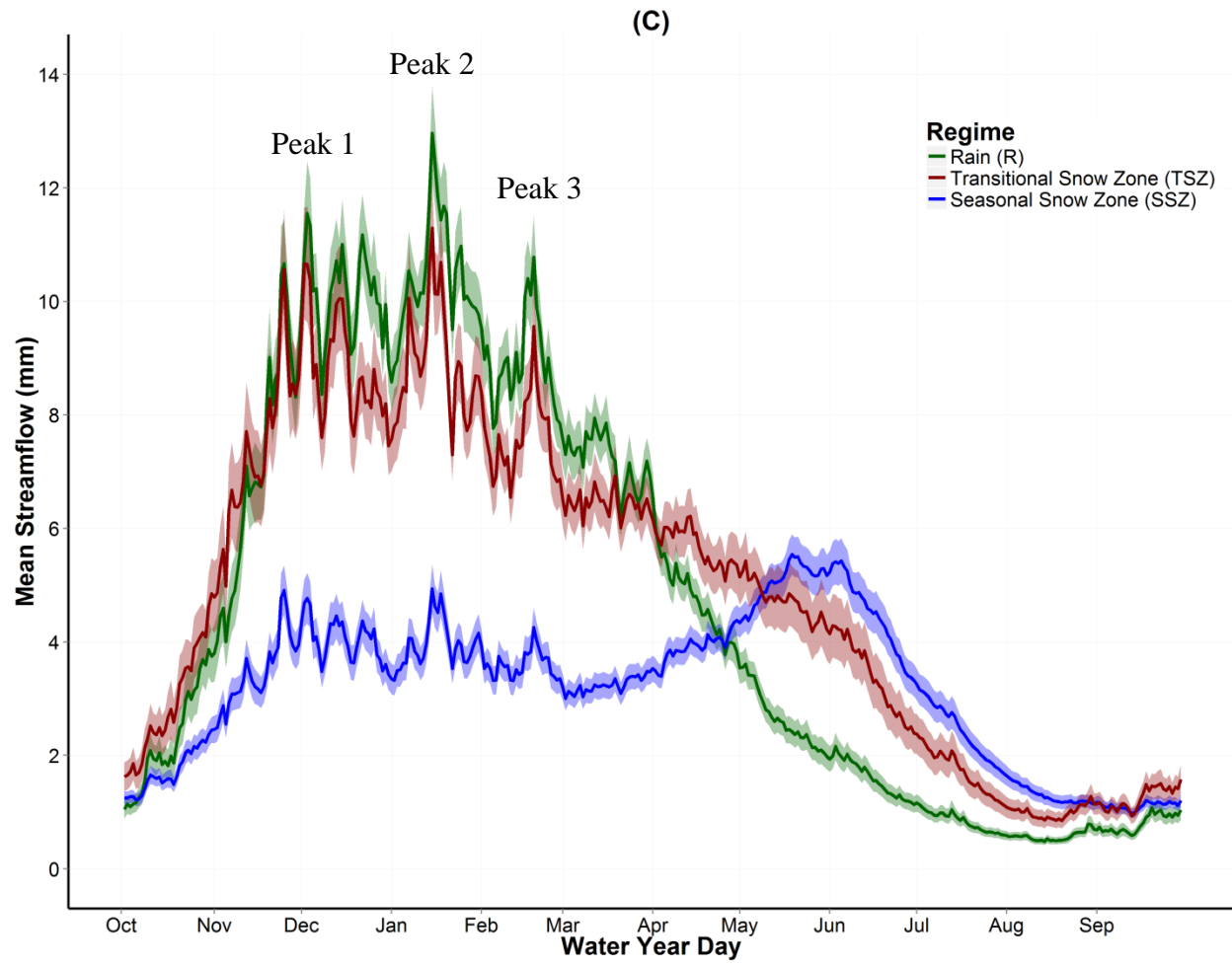
906

907



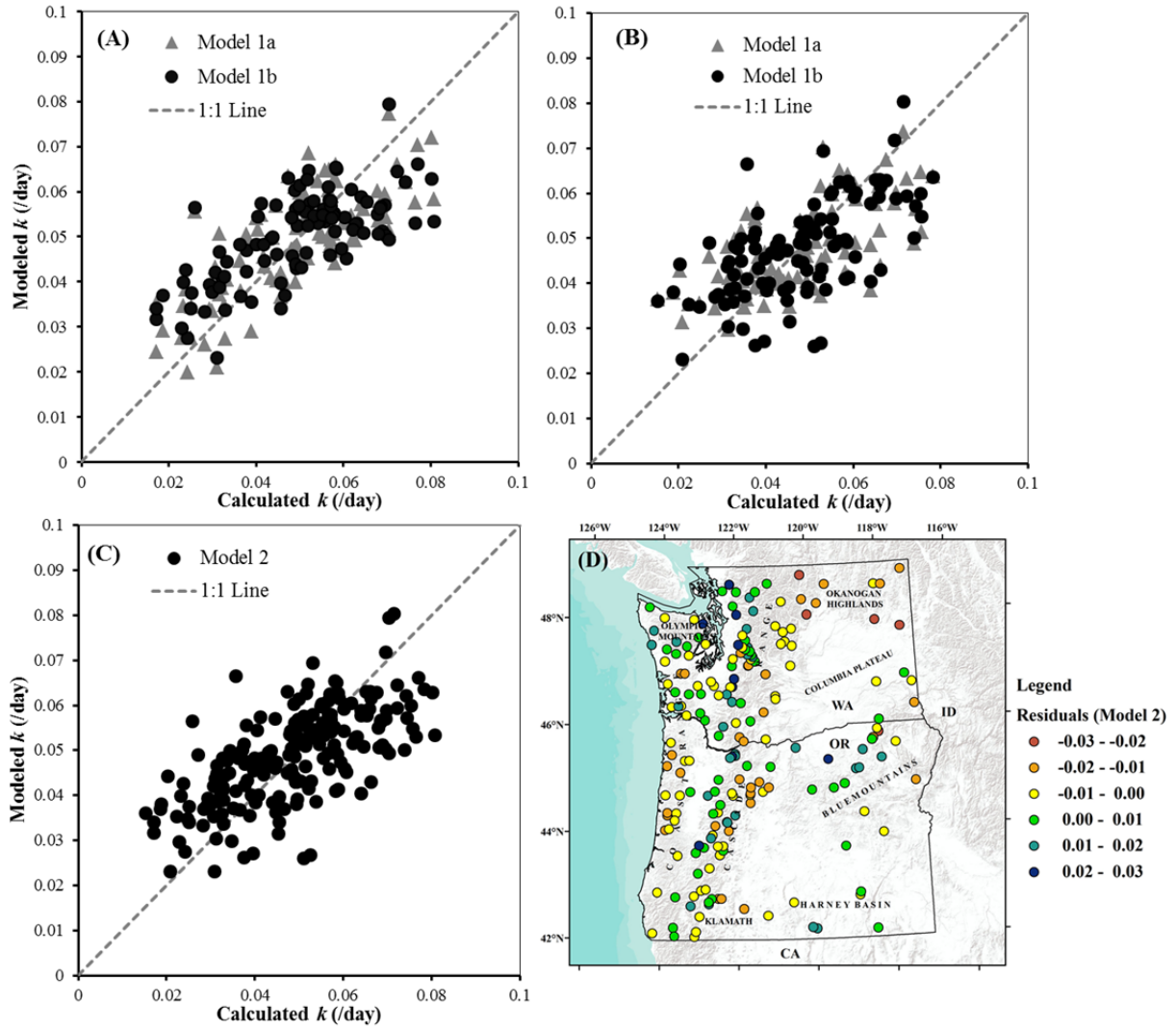
(B)





908 **Figure 3:** Time series of daily (1-365) rainfall (A), snowmelt (B), and streamflow (C) averaged
909 over the available lengths of record (1915-2006) and n watersheds in rain (R, $n = 44$; green),
910 transitional snow zone (TSZ, $n = 43$; red), and seasonal Snow zone (SSZ, $n = 130$; blue). Solid
911 lines represent the mean value and shaded areas represent the standard error of the mean.

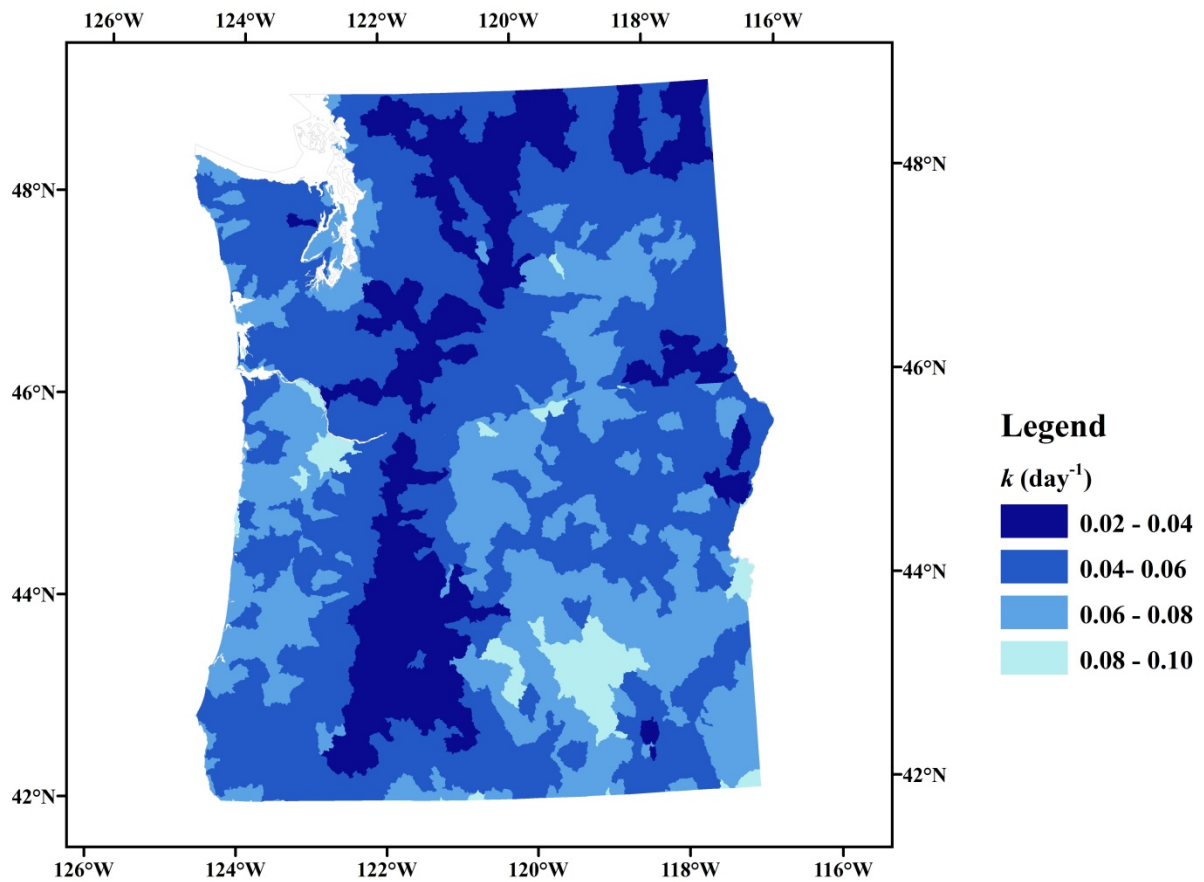
912



913

914 **Figure 4:** Calculated and modeled flow recession constant (k) for watersheds in (A) OR, (B)
 915 WA, and (C) entire domain based on the regression equations developed individually for OR
 916 (Model 1a), WA (Model 1b) and for the entire domain (Model 2); (D) Spatial distribution of
 917 residuals (Calculated-Modeled) using Model 2.

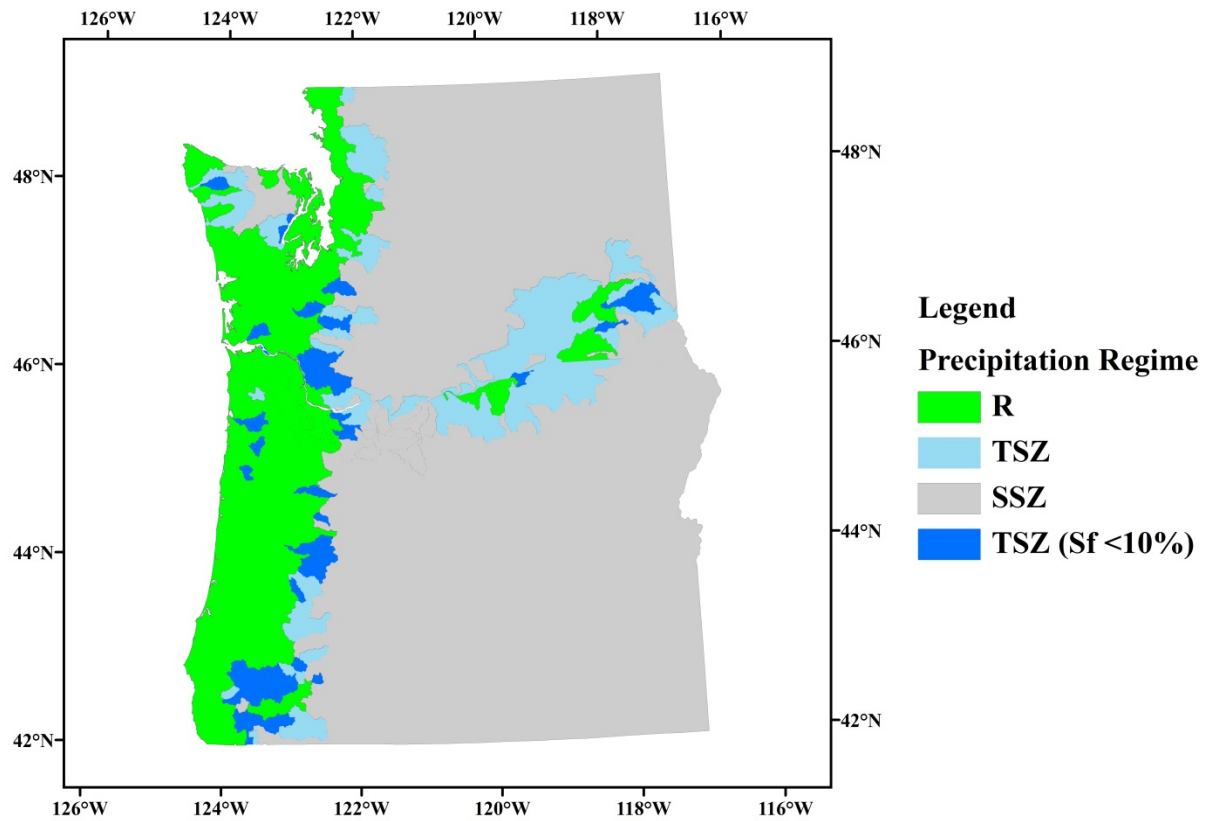
918



919

920 **Figure 5A:** Spatial distribution of recession constant k using Model 2 for the entire domain of
 921 Oregon and Washington. Lower k values represent deep groundwater-dominated systems; higher
 922 k values represent surface flow-dominated systems.

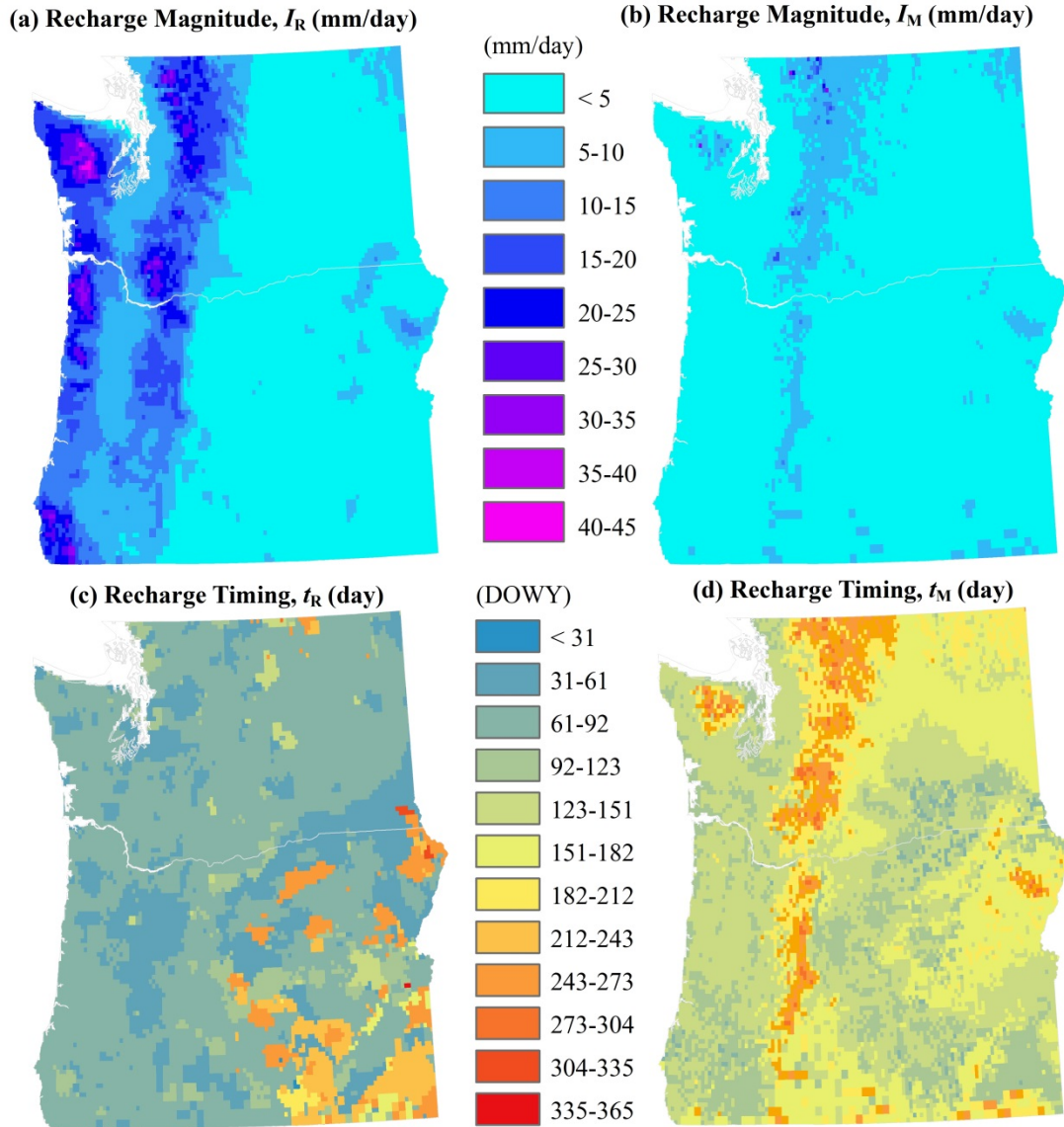
923



924

925 **Figure 5B:** Study domain discretized between rain (R; green), transitional snow zone (TSZ;
 926 blue), and seasonal snow zone (SSZ; gray) based on Nov-Jan average wet day air temperature.
 927 Areas in the TSZ with a snow to precipitation ratio (Sf) >10% are shaded with light blue.

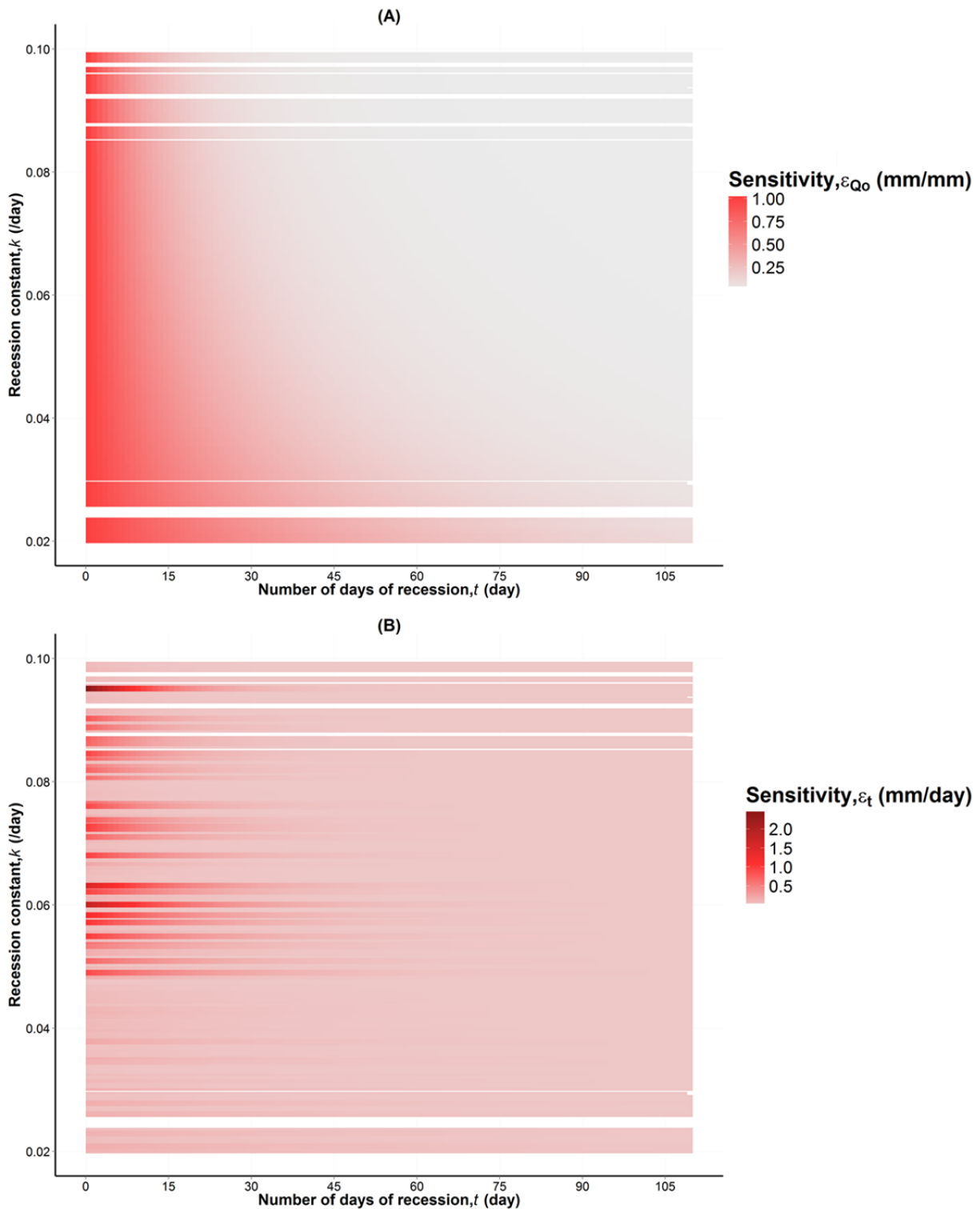
928



929

930 **Figure 6:** Spatial distribution of peak recharge magnitude (mm/day) for precipitation I_R (a),
 931 snowmelt I_M (b) and recharge timing (day of water year) for precipitation t_R (c) and snowmelt t_M
 932 (d) across the study domain.

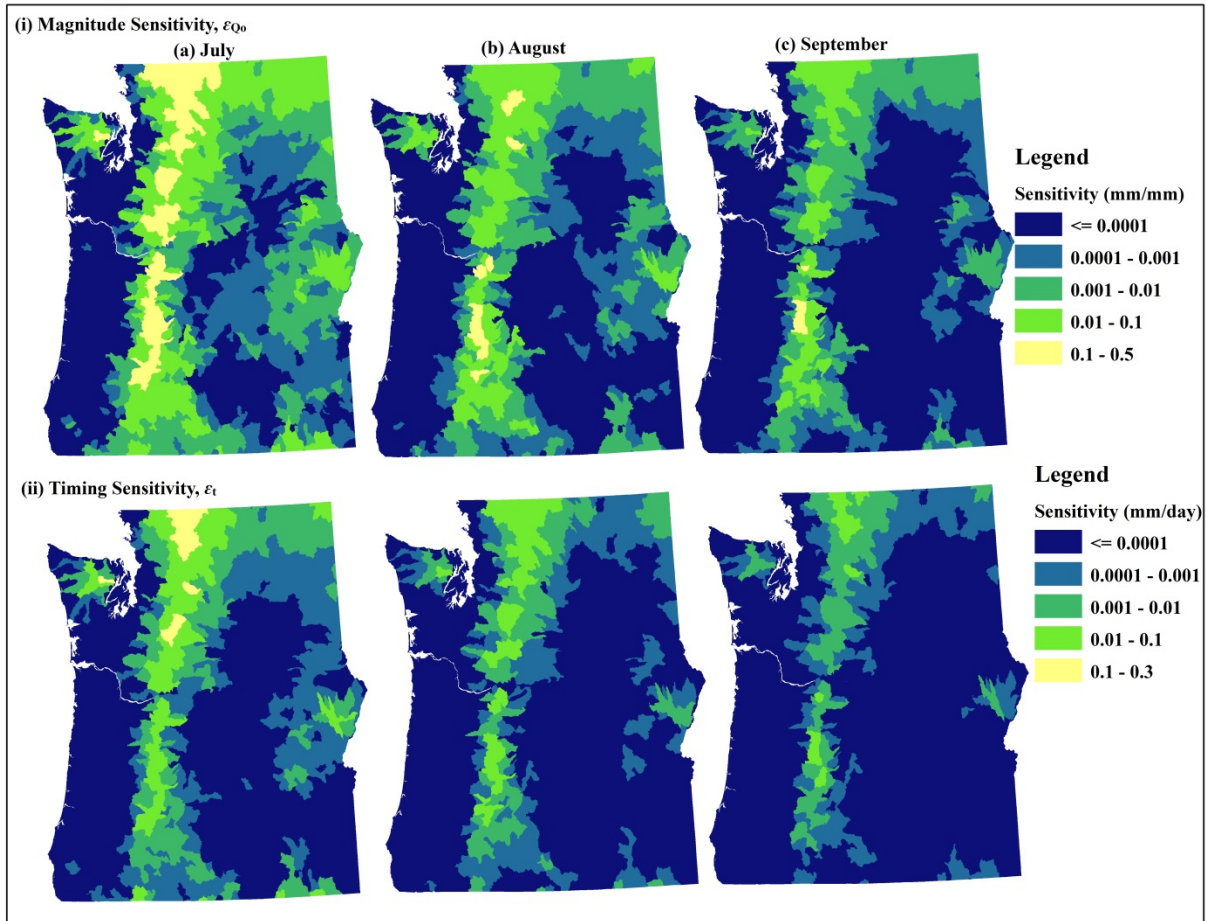
933



934

935 **Figure 7:** Decline of streamflow sensitivities for the range of k across all HUC units to a change
 936 in (A) magnitude, ϵ_{Q_0} and (B) timing, ϵ_t during the first 110 days of recession from the peak
 937 recharge, t_p . White shading indicates no data.

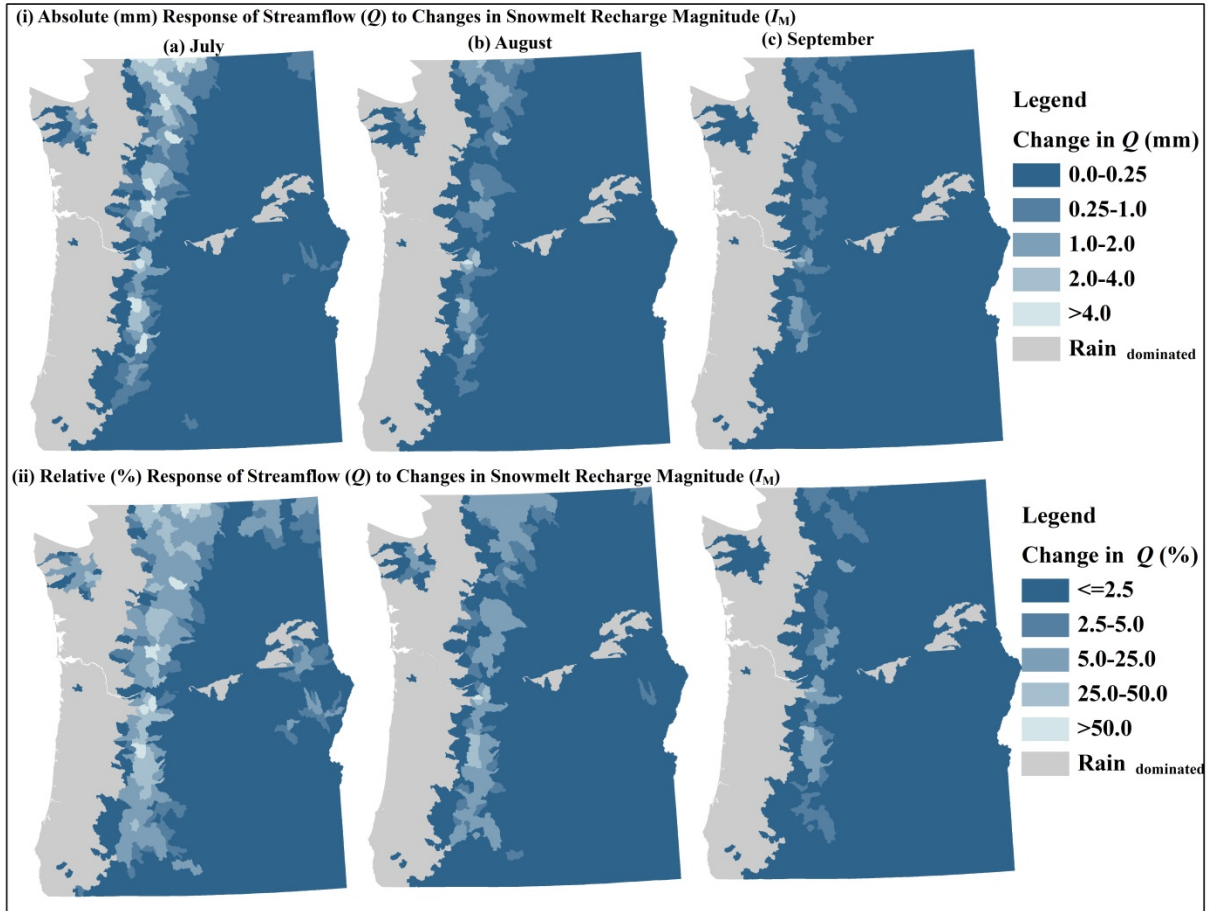
938



939

940 **Figure 8:** Spatial distribution of (A) July, (B) August and (C) September streamflow sensitivities
 941 to a change in (i) magnitude ϵ_{Q_0} (mm/mm) and (ii) timing ϵ_t (mm/day) of recharge.

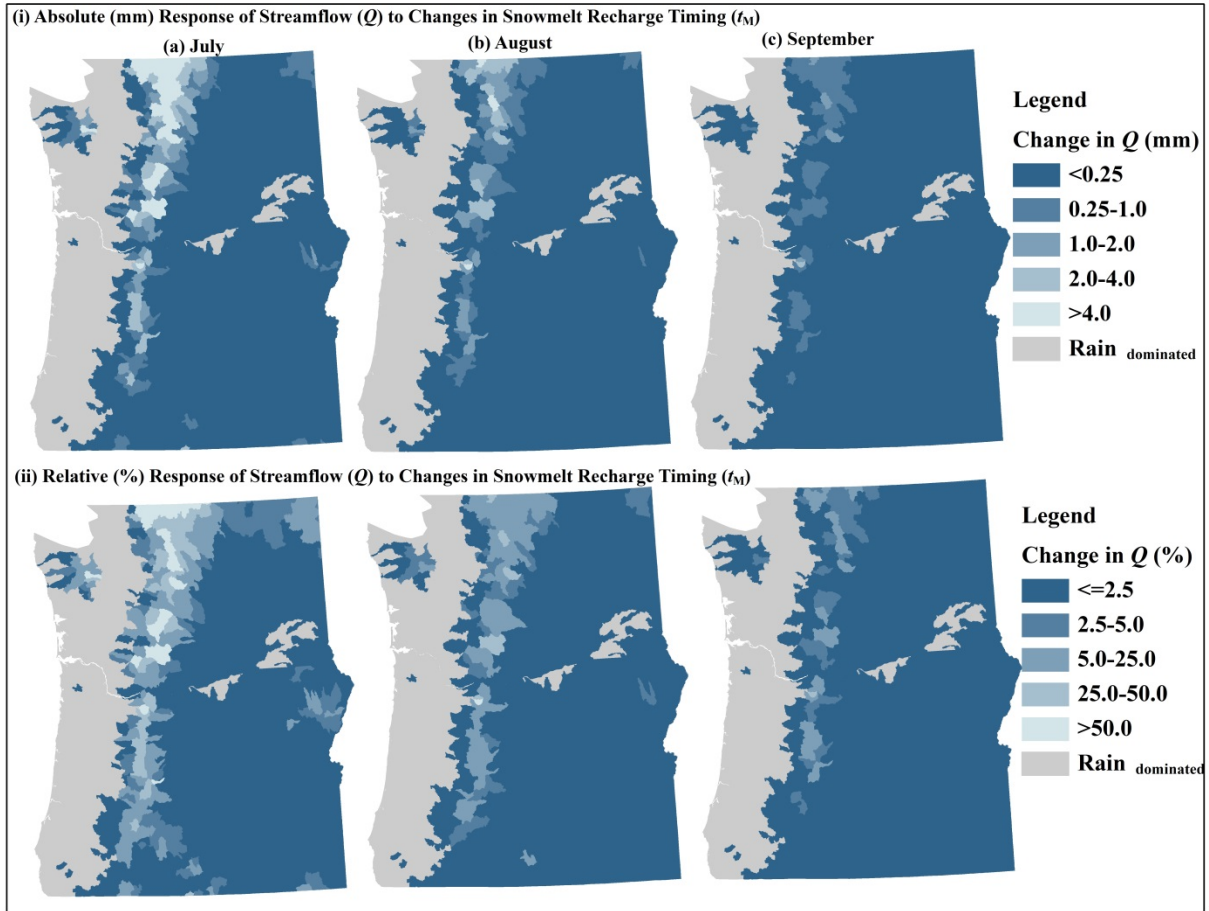
942



943

944 **Figure 9A:** Predicted decline in streamflow in absolute (i) and relative (ii) terms, based on: 1)
 945 the intrinsic sensitivities to changes in peak snowmelt magnitude (Fig. 8); and 2) a scenario
 946 similar to the differences experienced between a warm, dry year (2003, El Niño) and a cool, wet
 947 year (2011, La Niña). Gray areas are rain dominated recharge and were excluded from this
 948 analysis.

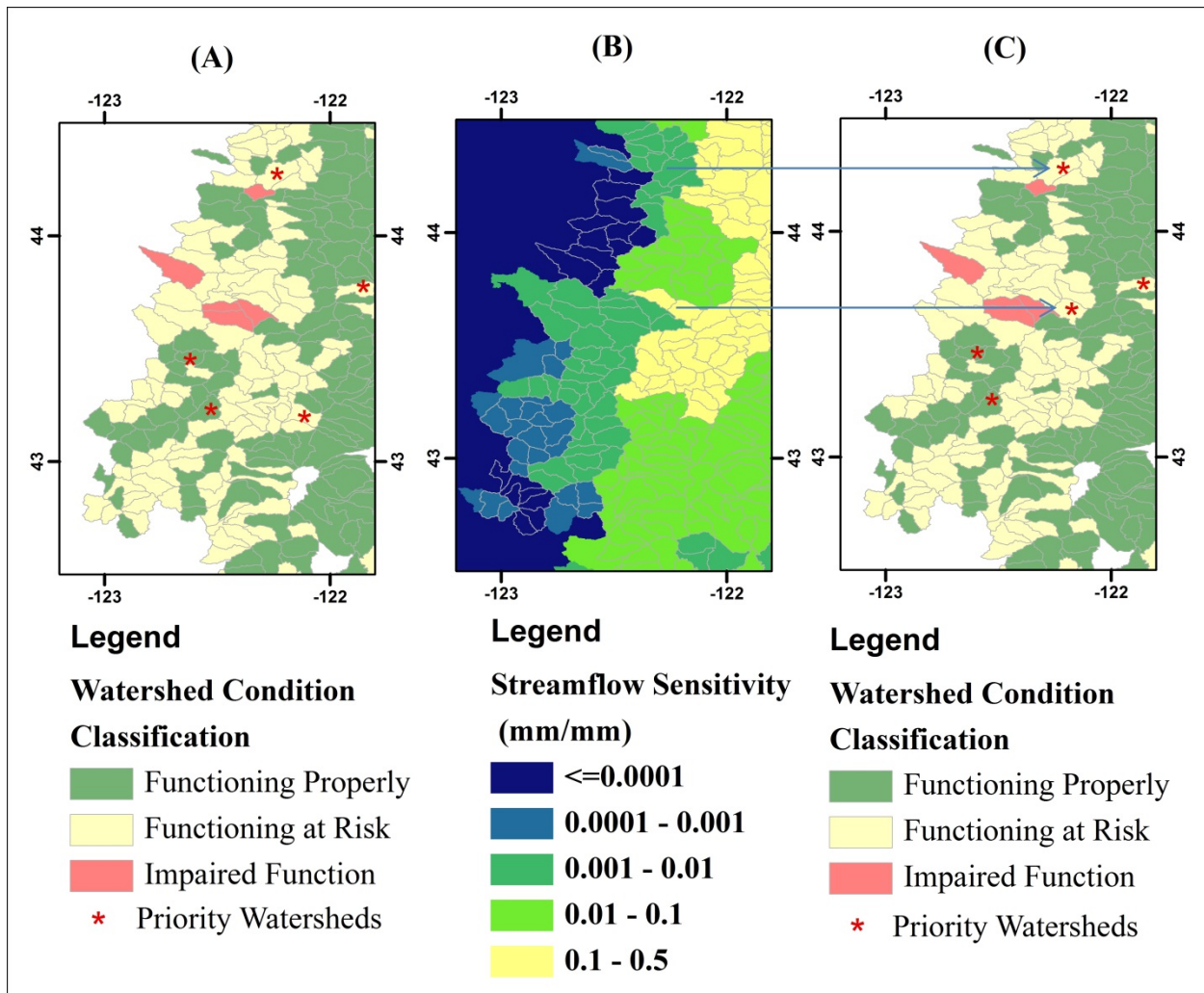
949



950

951 **Figure 9B:** Predicted decline in streamflow in absolute (i) and relative (ii) terms, based on: 1)
 952 the intrinsic sensitivities to changes in peak snowmelt timing (Fig. 8); and 2) a scenario similar
 953 to the difference experienced between a warm, dry year (2003, El Niño) and a cool, wet year
 954 (2011, La Niña). Gray areas are rain dominated recharge and were excluded from this analysis.

955



956

957 **Figure 10:** Examples of hypothetical watershed prioritization based on USDA Forest Service
 958 Watershed Condition Classification, an assessment of non-climatic impacts, sensitivities to those
 959 impacts, and opportunities to address them. Priority watersheds (red stars) differ for
 960 classifications without (A) and with (C) streamflow sensitivity analysis (B).

961